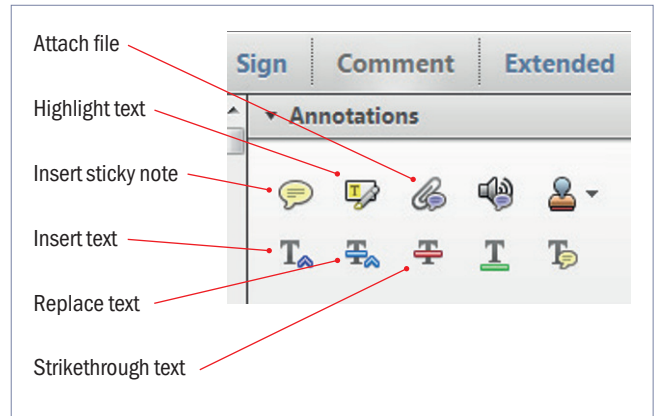


# Making corrections to your proof

Please follow these instructions to mark changes or add notes to your proof. You can use Adobe Acrobat Reader (download the most recent version from <https://get.adobe.com>) or an open source PDF annotator.

For Adobe Reader, the tools you need to use are contained in **Annotations** in the **Comment** toolbar. You can also right-click on the text for several options. The most useful tools have been highlighted here. If you cannot make the desired change with the tools, please insert a sticky note describing the correction.

Please ensure all changes are visible via the 'Comments List' in the annotated PDF so that your corrections are not missed.

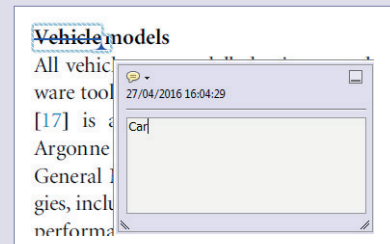


**Do not attempt to directly edit the PDF file as changes will not be visible.**



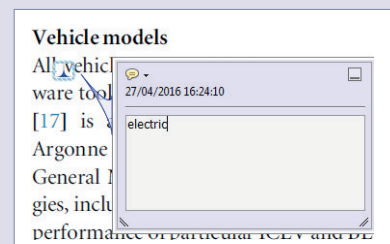
## Replacing text

To replace text, highlight what you want to change then press the replace text icon, or right-click and press 'Add Note to Replace Text', then insert your text in the pop up box. Highlight the text and right click to style in bold, italic, superscript or subscript.



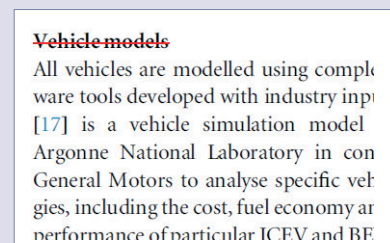
## Inserting text

Place your cursor where you want to insert text, then press the insert text icon, or right-click and press 'Insert Text at Cursor', then insert your text in the pop up box. Highlight the text and right click to style in bold, italic, superscript or subscript.



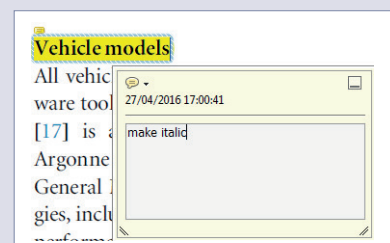
## Deleting text

To delete text, highlight what you want to remove then press the strikethrough icon, or right-click and press 'Strikethrough Text'.



## Highlighting text

To highlight text, with the cursor highlight the selected text then press the highlight text icon, or right-click and press 'Highlight text'. If you double click on this highlighted text you can add a comment.



# QUERY FORM

JOURNAL: Biofabrication

AUTHOR: D Gholobova et al

TITLE: Functional evaluation of prevascularization in one-stage versus two-stage tissue engineering approach of human bio-artificial muscle

ARTICLE ID: ab8f36

---

---

Your article has been processed in line with the journal style. Your changes will be reviewed by the Production Editor, and any amendments that do not comply with journal style or grammatical correctness will not be applied and will not appear in the published article.

The layout of this article has not yet been finalized. Therefore this proof may contain columns that are not fully balanced/matched or overlapping text in inline equations; these issues will be resolved once the final corrections have been incorporated.

Please check that the **names of all authors as displayed in the proof are correct**, and that **all authors are linked to the correct affiliations**. Please also confirm that the correct corresponding author has been indicated. **Note that this is your last opportunity to review and amend this information before your article is published.**

If an explicit acknowledgment of funding is required, please ensure that it is indicated in your article. If you already have an Acknowledgments section, please check that the information there is complete and correct.

Note that the supplementary data associated with your article will be hosted as supplied, and will not be processed by us. If you wish to supply new files, please send them along with your proof corrections.

---

We have been provided with ORCID iDs for the authors as below. Please confirm whether the numbers are correct.

L Thorrez <https://orcid.org/0000-0002-5896-6823>

---

## Page 16

Q1  
Please check the details for any journal references that do not have a link as they may contain some incorrect information. If any journal references do not have a link, please update with correct details and supply a Crossref DOI if available.

---

## Page 16

Q2  
Reference [19] is a duplicate of [12] and hence the repeated version has been deleted. Please check.

---

## Page 17

Q3  
Please provide the volume number in references [25, 31].

# Biofabrication



## PAPER

### OPEN ACCESS

RECEIVED  
13 July 2019

REVISED  
6 March 2020

ACCEPTED FOR PUBLICATION  
1 May 2020

PUBLISHED  
xx xx xxxxx

Original content from this work may be used under the terms of the [Creative Commons Attribution 3.0 licence](https://creativecommons.org/licenses/by/4.0/).

Any further distribution of this work must maintain attribution to the author(s) and the title of the work, journal citation and DOI.



# Functional evaluation of prevascularization in one-stage versus two-stage tissue engineering approach of human bio-artificial muscle

D Gholobova<sup>1</sup>, L Terrie<sup>1</sup>, K Mackova<sup>2,3,4,5</sup>, L Desender<sup>1</sup>, G Carpentier<sup>6</sup>, M Gerard<sup>1</sup>, L Hympanova<sup>2,3,4,5</sup>, J Deprest<sup>2,3,4</sup> and L Thorrez<sup>1</sup>

<sup>1</sup> Tissue Engineering Lab, Department of Development and Regeneration, KU Leuven, E. Sabbelaan 53, 8500, Kortrijk, Belgium

<sup>2</sup> Centre for Surgical Technologies, Group Biomedical Sciences, KU Leuven, Leuven, Belgium

<sup>3</sup> Department of Development and Regeneration, Woman and Child, Group Biomedical Sciences, KU Leuven, Leuven, Belgium

<sup>4</sup> Pelvic Floor Unit, University Hospitals KU Leuven, Leuven, Belgium

<sup>5</sup> Institute for the Care of Mother and Child, Third Faculty of Medicine, Charles University, Prague, Czech Republic

<sup>6</sup> Laboratoire de Recherche sur la Croissance Cellulaire, la Réparation et la Régénération Tissulaires (CRRET), Faculté des Sciences et Technologie, Université Paris-Est, 94000, Créteil, France

E-mail: [lieven.thorrez@kuleuven.be](mailto:lieven.thorrez@kuleuven.be)

**Keywords:** prevascularization, tissue engineering, skeletal muscle

Supplementary material for this article is available [online](#)

## Abstract

A common shortcoming of current tissue engineered constructs is the lack of a functional vasculature, limiting their size and functionality. Prevascularization is a possible strategy to introduce vascular networks in these constructs. It includes among others co-culturing target cells with endothelial (precursor) cells that are able to form endothelial networks through vasculogenesis. In this paper, we compared two different prevascularization approaches of bio-artificial skeletal muscle tissue (BAM) *in vitro* and *in vivo*. In a one-stage approach, human muscle cells were directly co-cultured with endothelial cells in 3D. In a two-stage approach, a one week old BAM containing differentiated myotubes was coated with a fibrin hydrogel containing endothelial cells. The obtained endothelial networks were longer and better interconnected with the two-stage approach. We evaluated whether prevascularization had a beneficial effect on *in vivo* perfusion of the BAM and improved myotube survival by implantation on the fascia of the *latissimus dorsi* muscle of NOD/SCID mice for 5 or 14 d. Also *in vivo*, the two-stage approach displayed the highest vascular density. At day 14, anastomosis of implanted endothelial networks with the host vasculature was apparent. BAMs without endothelial networks contained longer and thicker myotubes *in vitro*, but their morphology degraded *in vivo*. In contrast, maintenance of myotube morphology was well supported in the two-stage prevascularized BAMs. To conclude, a two-stage prevascularization approach for muscle engineering improved the vascular density in the construct and supported myotube maintenance *in vivo*.

## 1. Introduction

Skeletal muscle tissue has a high regenerative capacity that is able to replace damaged muscle tissue upon injury [1, 2]. A central role in muscle regeneration is played by the muscle progenitor cells known as satellite cells. However in cases of volumetric muscle loss, a failure of muscle repair and scar tissue formation is often observed, resulting in functional muscle impairment [2]. The current treatment strategy for localized skeletal muscle repair includes muscle flap

transplantation. Therefore, autologous muscle tissue is transplanted from a donor site to the damaged muscle. Unfortunately, this is associated with donor site morbidity and poor flap survival [3]. To limit this problem, microsurgery is used to include vasculature to allow the reconstitution of blood supply in the tissue. In turn, this provides oxygen and nutrients, and removes waste products throughout the transplanted tissue [4, 5].

To avoid the need of donor site tissue and related injuries, tissue engineered skeletal muscle

holds promise as an alternative treatment. Skeletal muscle tissue engineering aims to create *in vitro* muscle tissue that mimics the structure and function of *in vivo* muscle, and thus offers the potential to repair the damaged muscle area. Similar to muscle flaps, one of the current limitations of avascular tissue engineered constructs is the lack of a blood supply in the initial phase after implantation since passive diffusion is limited to 150–200  $\mu\text{m}$  [4, 6, 7]. In response to the hypoxia that arises when having a tissue engineered graft with wall thickness greater than the diffusion limit, host vessels invade the implanted tissue. However, the rate of spontaneous vascular ingrowth is limited to  $\sim 5 \mu\text{m h}^{-1}$  [8], which cannot address the metabolic need in time leading to necrosis in the central area of the graft. As a result, successful use of tissue-engineered constructs in the clinic is limited to thin or avascular tissues, such as skin or cartilage, in which this rate of neovascularization from the host is sufficient. Yet, in other tissue grafts such as muscle, vascularization will be of key importance to achieve successful transplantation. This remains an important hurdle to overcome if the aim is to increase the size of engineered tissue constructs as the lack of oxygen and nutrient supply constrains the size of viable constructs.

Prevascularization is the formation of capillary-like networks before implantation and is aimed to overcome this diffusion limit. As for engineering (immature) blood vessels in skeletal muscle constructs, a few *in vitro* approaches have been described, such as co-culturing endothelial cells (EC) and myogenic progenitors on different scaffolds and hydrogels, combining endothelial cell sheets with myoblast cell sheets and engineering vasculature using microfabrication techniques [4, 5, 9, 10]. Besides applications in regenerative medicine, such a vascularized muscle model can be used to study mechanisms underlying myogenesis, vasculogenesis and vasculomyogenic interactions.

This prevascularization is based on *de novo* blood vessel formation known as vasculogenesis and the advantages of this strategy are fourfold. First, the presence of this preformed endothelial network further enhances host vessel ingrowth upon implantation [11, 12]. Second, having a prevascularized construct bears the advantage that the preformed microvascular network only has to anastomose to the host vasculature after implantation to achieve rapid construct vascularization [13]. Third, this prevascularization improves perfusion and survival of the construct upon implantation [11, 12]. Fourth and last, in addition to forming blood vessels, endothelial cells are known for their paracrine activity on developing tissue, including skeletal muscle [14–16]. Although an *in vitro* prevascularization approach reduces the time needed for complete vascularization, perfusion is not as fast as with *in vivo* prevascularization using microsurgery to connect the construct to

the host vasculature. However, vascularization speed is not the sole factor to consider [16]. Functionality of the newly formed vessels will determine the success of a tissue-engineering strategy as well. More specifically, regression of *in vitro* formed networks should be avoided [17].

Still, only a limited number of implantation studies focused on pre-vascularized tissue engineered skeletal muscle have been conducted so far. A prevascularized fibrin matrix, obtained using a microsurgically created arteriovenous-loop approach, was injected with expanded primary myoblasts [18]. This prevascularization approach promoted myoblast survival and preservation of the myogenic phenotype, but no differentiation into myotubes occurred. In another approach, a prevascularized construct containing HUVECs (human umbilical vein endothelial cells), C2C12 mouse myoblasts and fibroblasts was implanted, which resulted in enhanced survival and prolonged functionality of the skeletal muscle construct [12, 19]. The used poly-L-lactic acid (PLLA)/poly(lactic-glycolic acid) (PLGA) 3D porous scaffolds however over time release acidic degradation products, which decrease cell survival [20]. Thus, this approach may not represent the most optimal approach for tissue engineering vascularized skeletal muscle. Similarly, an engineered flap composed of human adipose-derived microvascular endothelial cells and mesenchymal stem cells seeded on the same PLLA/PLGA scaffold was used for abdominal wall defect repair [21]. The graft was cultured *in vitro* until a small capillary net was formed. This was folded around an exposed femoral artery and vein of the recipient rat. After 21 d, the grafts with the arteries and veins were transferred to an abdominal full-thickness wall defect. This resulted in a highly vascularized, well-integrated muscle flap. However, further reports on functional muscle regeneration using this approach are missing.

Another disadvantage in the above mentioned prevascularization studies is the use of solid scaffolds. The skeletal muscle tissue-engineering approach used in our lab is based on previous work of the Vandenberg lab and uses hydrogels, allowing cells to self-organize and migrate [22, 23]. In addition, a hydrogel better mimicks the physiological environment of developing skeletal muscle which has been shown to influence the proliferation of muscle progenitor cells [24]. In this approach, cells isolated from a human muscle biopsy are expanded to several millions of muscle cells (myoblasts and a minority of fibroblasts). These are cast in silicone molds in the presence of a natural hydrogel. After one week, this results in the formation of a bio-artificial muscle (BAM) containing multinucleated myotubes, well-aligned in the direction of the attachment points. The BAM is limited in size (2 cm long,  $\pm 1$  mm thick) due to the absence of a vascular network. To increase the size of the BAM, which would expand its applications

and utility, we already succeeded in prevascularizing a BAM *in vitro* in a previous study [10]. This was done by seeding HUVECs together with muscle cells in a fibrin hydrogel followed by one week of tissue contraction and cell differentiation. This is a direct 3D co-culture approach, defined as a one-stage prevascularization approach in this manuscript (BAM-1s). Despite detailed *in vitro* analysis, our previous study lacked an *in vivo* part in which the functionality of the preformed endothelial networks was tested. In this follow-up study we aim to (i) further improve the prevascularization with minimal loss of myotube formation in the BAM based on a novel two-stage BAM prevascularization approach (BAM-2s) and (ii) assess *in vivo* behaviour of prevascularized BAMs in a mouse model.

## 2. Methods

### 2.1. Cell culture media

The medium that was employed for the isolation and proliferation of myogenic progenitors (skeletal muscle growth medium, SkGM) was composed of high glucose Dulbecco's Modified Eagle Medium (DMEM, Gibco), 10% fetal bovine serum (FBS, Thermo Fisher), 50  $\mu\text{g ml}^{-1}$  gentamicin (Life Technologies), and 1% Ultrosor solution (Pall corporation). Differentiation medium (SkFM) composed of DMEM with high glucose containing 10  $\text{ng ml}^{-1}$  hEGF, 10  $\mu\text{g ml}^{-1}$  insulin, 50  $\mu\text{g ml}^{-1}$  BSA and 50  $\mu\text{g ml}^{-1}$  gentamicin was used to promote formation of multinucleated myotubes.

### 2.2. Cell culture

Green Fluorescent Protein (GFP)-labeled HUVECs (GFP-HUVECs, Angio-proteomie) were seeded in cell culture flasks which were precoated for 1 h at 37 °C with gelatin (0.1% gelatin, Millipore) and cultured in endothelial growth medium (EGM-2 with bullet kit, Lonza). HUVECs were split at 90% confluence and used in the experiment at passage 7.

Human skeletal muscle cells were isolated from a fresh human muscle tissue biopsy, of an adult male aged 60, obtained from the Human Body Donation programme of KU Leuven University as described in [25]. The donor provided written consent (for research and educational purpose) prior to death. Briefly, isolated tissue was cut in strips of approximately 2 mm  $\times$  10 mm using sterile forceps and scalpel after removing excess connective tissue and fat. Before isolation of cells, muscle strips were pinned under tension into a sylgard coated 6-well plate to maintain cell survival while avoiding muscle atrophy. Two days after pinning the strips, enzymatic digestion was performed by incubating the muscle strips at 37 °C for 1 h in DMEM high glucose with Glutamax and pyruvate supplemented with 0.1% collagenase, type II (Sigma) and 4  $\text{mg ml}^{-1}$  dispase II (Roche Diagnostics). After the incubation, isolated

cells were collected by filtering through a 100  $\mu\text{m}$  cell strainer (Falcon) and fragments were incubated again to digest the whole tissue. Isolated cells were pooled, centrifuged for 5 min at 200  $\times$  g and resuspended in SkGM. Muscle cells were split at 60%–70% confluence and used in experiments at 12 doublings. In the isolated muscle cell population, myoblast percentage and fusion index were determined as described before [10, 25].

Muscle cells that were used for tissue engineering of BAMs, and subsequently for implantation, expressed the far-red fluorescent protein miRFP670 [26]. The expression of miRFP670 was obtained by transducing 5  $\times$  10<sup>5</sup> muscle cells in 3.15 ml SkGM for 48 h with 350  $\mu\text{l}$  1.21  $\times$  10<sup>6</sup> pg p24 ml<sup>-1</sup> CMV-miRFP670 cDNA-containing HIV1-derived retroviral particles. Retroviral vectors were produced as previously described by the Leuven Viral Vector Core (Full description in [27] and with improvements in [28]). The transfer plasmid pCH-CMV-miRFP670-3xflag-IRES-blasti was made by cloning the miRFP670 sequence (RefSeq KX421097.1) into a pCH-CMV-eGFP-3xflag-Ires-blasti plasmid. All cloning steps were verified by sequencing. This resulted in the expression of triple flag-tagged miRFP670 under the control of a cytomegalovirus (CMV) promoter and with simultaneous expression of a blastidicin resistance cDNA. Lentiviral vector particle number was estimated by quantifying the surface protein p24 with enzyme linked immunosorbent assay (ELISA) (HIV-1 core profile ELISA, DuPont), which was determined to be 1.21  $\times$  10<sup>6</sup> pg p24 ml<sup>-1</sup>.

### 2.3. Tissue-engineering of BAMs

Three different types of BAMs were used: (i) BAMs containing only muscle cells (2 $\times$ 10<sup>6</sup> muscle cells construct<sup>-1</sup>) cultured for 2 weeks in SkGM/SkFM (termed BAM), (ii) the one-stage prevascularized BAM with muscle cells and endothelial cells (1.4 $\times$ 10<sup>6</sup> muscle cells and 0.6  $\times$  10<sup>6</sup> HUVECs construct<sup>-1</sup>) cultured for 1 week in EGM-2 (termed BAM-1s) and (iii) the two-stage prevascularized BAM with initially only muscle cells (2 $\times$ 10<sup>6</sup> muscle cells construct<sup>-1</sup>) cultured for 1 week in SkGM/SkFM followed by an additional embedding step in a fibrin hydrogel containing 2  $\times$  10<sup>6</sup> GFP labeled HUVECs (termed BAM-2s) (schematic representation in figure 1). In previous experiments, the initial seeding density of in total 2  $\times$  10<sup>6</sup> cells has been set based on the obtained alignment and dense formation of myofibers [10]. For the BAM-1s, this same initial cell density appeared to result in best myofiber formation and the total amount of cells was divided over the two cell types. The ratio of cells used was described to be the best trade-off between maximal myogenesis while having interspersed endothelial networks in [10]. Finally, for the BAM-2s the initial amount of cells (muscle cells) was kept constant (2 $\times$ 10<sup>6</sup>) as this allows the direct comparison with

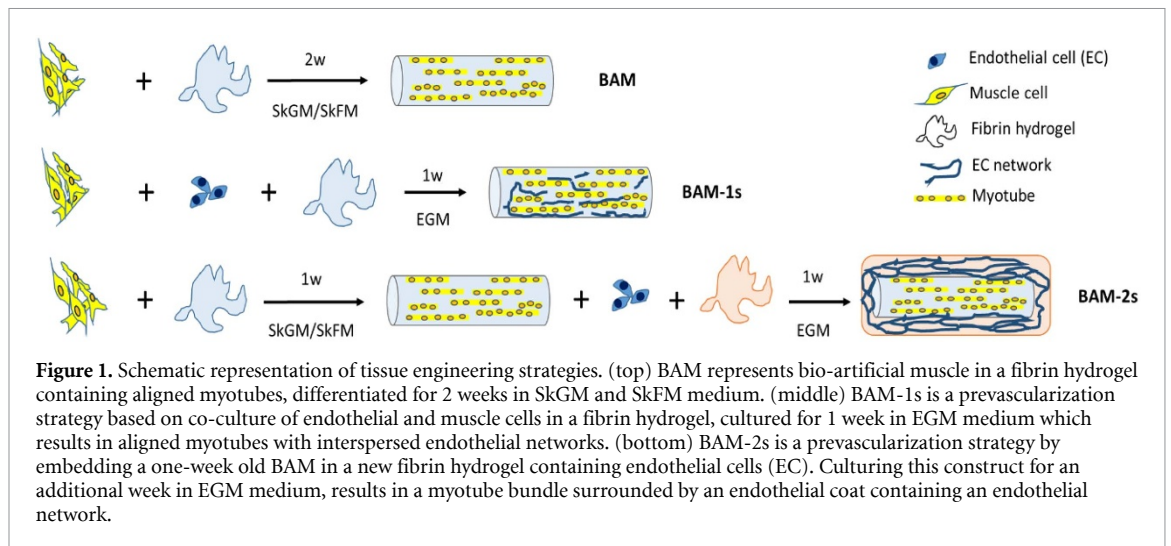


**Figure 1.** Schematic representation of tissue engineering strategies. (top) BAM represents bio-artificial muscle in a fibrin hydrogel containing aligned myotubes, differentiated for 2 weeks in SkGM and SkFM medium. (middle) BAM-1s is a prevascularization strategy based on co-culture of endothelial and muscle cells in a fibrin hydrogel, cultured for 1 week in EGM medium which results in aligned myotubes with interspersed endothelial networks. (bottom) BAM-2s is a prevascularization strategy by embedding a one-week old BAM in a new fibrin hydrogel containing endothelial cells (EC). Culturing this construct for an additional week in EGM medium, results in a myotube bundle surrounded by an endothelial coat containing an endothelial network.

the BAM in terms of myofibers while endothelial cell numbers were increased to  $2 \times 10^6$  HUVECs. The latter was optimized separately in terms of maximal endothelial network formation extent.

Tissue-engineering of BAMs was described in [10, 25]. Briefly, cells were mixed with  $500 \mu\text{l}$  thrombin ( $4 \text{ U ml}^{-1}$ , Bio Phar Laboratories LLC). The mixture was cast into 25-mm-long silicone rubber molds with end attachment sites spaced 20 mm. Then, to form a fibrin hydrogel ( $1 \text{ mg ml}^{-1}$ ) containing the cells,  $500 \mu\text{l}$  fibrinogen ( $2 \text{ mg ml}^{-1}$ , Merck Chemicals) was added and the cell-gel mix was mixed. Following 2 h incubation at  $37^\circ\text{C}$ , SkGM (for BAM) or EGM-2 medium (for BAM-1s) supplemented with fibrinolysis inhibitors aprotinin ( $92.5 \mu\text{g ml}^{-1}$  Carl Roth) and tranexamic acid ( $400 \mu\text{M}$ , Sigma) was added. For BAM, the medium was switched to differentiation medium (SkFM) two days after casting. To obtain the third type of BAM, BAM-2s, 1 week old BAMs were embedded in 1 ml fibrin (created similar as above) hydrogel containing  $2 \times 10^6$  HUVECs and cultured for another week in EGM-2. Medium was replaced every 2 d and BAMs were kept in culture for 7 or 14 d prior to thickness measurement and fixation.

#### 2.4. Thickness measurements

Cross-sectional thickness of BAMs in culture and post-implantation was measured with a sterile micrometer at day 7 or day 14 after casting.

#### 2.5. *In vivo* implantation of BAMs

All animal experiments were evaluated and approved by the Animal Ethics Committee of the KU Leuven (P099/2017) and were performed according to international guidelines. BAMs were implanted subcutaneously on the fascia of the *latissimus dorsi* muscle for a period of 14 d in 6–7 weeks old non-obese diabetic severe combined immunodeficiency (NOD/SCID) mice (Janvier) ( $n = 12$  for BAM,  $n = 8$  for BAM-1s and  $n = 4$  for BAM-2s). Imbalance

in numbers is related to the surgical procedure in which a lower number of animals with the BAM-2s constructs survived. The higher number of the BAM as compared to the BAM-1s and BAM-2s is because the BAM condition was used as a reference in each animal. All animals were anesthetized and maintained with isoflurane ( $0.5\text{--}2\%$ ,  $3\text{--}5 \text{ l min}^{-1}$ ) and oxygen while being kept warm on a heating pad during surgery and recovery. The fascia of the *latissimus dorsi* muscle was scraped with a sterile scalpel until minor bleeding was observed. Both sides of the BAM were secured to the muscle with non-resorbable polypropylene suture (Ethicon) parallel to the spine. After implantation, meloxicam ( $2 \text{ mg kg}^{-1}$ ; Meloxidyl CEVA) and buprenorphine ( $0.1 \text{ mg kg}^{-1}$ ; Vetergesic) (for 2 d) were administered subcutaneously. Animals were euthanized 5 or 14 d later. Construct and underlying host tissue were explanted to capture both construct maintenance and host vessel ingrowth as well as construct integration into the host respectively. Host muscle without direct contact with the implanted constructs (gastrocnemius) was explanted each time and served as a negative control for all graft-specific stainings. Explants were washed in PBS for 5 min and fixed using 4% formaldehyde solution (w/v) for 6 h at room temperature (RT).

#### 2.6. Whole mount immunofluorescence staining

To assess *in vitro* BAM formation, the 3 types of BAM (BAM, BAM-1s, BAM-2s) were washed ( $3 \times 5 \text{ min}$  in PBS) and then removed from the attachment sites. Then, they were pinned on Styrofoam to preserve their original shape during fixation in 4% formaldehyde for 1 h at room temperature (RT) and stored at  $4^\circ\text{C}$  in PBS. Explanted constructs from the *in vivo* implantation study were fixed for 6 h at RT in 4% formaldehyde and stored at  $4^\circ\text{C}$  in PBS in the dark. For tropomyosin immunohistochemical staining, samples were fixed a second time, in methanol ( $-20^\circ\text{C}$ , 20 min) immediately prior to staining.

Next, the samples were permeabilized in blocking buffer containing 0.2% Triton-X-100 (Sigma) and 1% bovine serum albumin (BSA, Sigma) in PBS for 3 h at RT. Subsequently, the samples were incubated overnight at 4 °C with a monoclonal mouse antibody against tropomyosin (Sigma, T9283, 1:100 in blocking buffer) or with polyclonal rabbit antibody against collagen IV (Abcam, ab6586, 1:400 in blocking buffer). To stain capillaries, the explanted BAM constructs were incubated overnight at 4 °C with a polyclonal rabbit antibody against CD 31 (Invitrogen, PA16301, 1:30 in blocking buffer). Next, the human BAMs and explants were washed and incubated with a polyclonal goat anti-mouse secondary antibody (Alexa Fluor 633, A-11 059 or A-21 063, Invitrogen, 1:200), a polyclonal goat anti-rabbit secondary antibody (Alexa Fluor 633, A21070, Thermo Fisher) or a polyclonal donkey anti-rabbit secondary antibody (Alexa Fluor 488, A-21 206, Life Technologies) for 3 h in the dark, followed by incubation with DAPI (Life Technologies, 0.1  $\mu\text{g ml}^{-1}$  in PBS) for 1 h at RT. Samples were stored in PBS in the dark until visualized.

### 2.7. Confocal imaging

Confocal imaging and data analysis of *in vitro* BAMs and *in vivo* BAMs were performed as described in [10]. Briefly, BAMs and explanted tissue were visualized by confocal microscopy (Zeiss LSM710). Per BAM, 5 z-stacks were acquired with Plan-Apochromat 25x/0.8, WD 0.57 mm objective every 5  $\mu\text{m}$ . Since explanted BAMs at day 14 were surrounded by host tissue, the distance to the construct exceeded the working distance of the objective. Therefore, explanted tissue was embedded in liquid 4% agarose in distilled water, cooled until the agarose solidified and cut in 200  $\mu\text{m}$  sections using a vibratome (Microm HM 650 V, VWR) to allow visualization within the whole explanted tissue (in collaboration with Prof. Veerle Baekelandt, KU Leuven). More detailed images were acquired with Plan-Apochromat 63x/1.2, WD 0.49 mm. Three dimensional reconstructions of stacked images were generated with Imaris 9.2.0 software (Bitplane).

### 2.8. Histology

4% formaldehyde fixed BAMs and explanted constructs were dehydrated through an alcohol series and embedded in paraffin. Tissue was sectioned at a thickness of 5  $\mu\text{m}$  with a microtome (Leica RM2125 RTS). Tissue slices were stained with Martius Scarlet Blue (MSB) staining [29] to evaluate the extracellular matrix deposition in BAMs before and after implantation. Murine muscle was used as positive control.

### 2.9. Data analysis

Myotube analysis and endothelial network analysis in *in vitro* constructs and after implantation were

performed as previously reported in Gholobova *et al* [10]. For myotube formation 20  $\mu\text{m}$  z-projections were manually analyzed for different parameters of myotube formation: myotube alignment, length, density and diameter. Myotube alignment was represented as the mean of the standard deviation of the angles of the myotubes. A lower number thus indicates better alignment. For endothelial network analysis, 60  $\mu\text{m}$  z-projections were automatically analyzed by a customized version of the 'Angiogenesis Analyzer', an ImageJ plugin created by Gilles Carpentier [10, 30]. Moreover, a customized algorithm was developed that was able to detect non-perfused and perfused vessels. This tool is able to measure several parameters of endothelial networks of which we used: total length of endothelial network (master segments, branches and isolated segments), % master segments (length of master segments, longest elements giving origin to branches, divided by total network length), % branching length (length of interconnected segments and branches, elements delimited by two junctions, or a junction and one extremity, divided by total network length) and % isolated segments (length of isolated segments, binary lines which are not branched, divided by total network length).

### 2.10. Detection of anastomosis

Two different approaches were used to evaluate anastomosis and perfusion of the implanted endothelial networks with host vessels; in the first approach 1.25  $\mu\text{g g}^{-1}$  body mass rhodamine-labelled Ulex europaeus agglutinine-I (UEA-I; Vectorlabs) was injected intravenously in the tail vein, circulation was allowed for 2 min, whereafter the animal was euthanized by cervical dislocation. UEA-I specifically targets human endothelial cells. Presence of UEA-I positive human endothelial networks was confirmed with confocal imaging of explanted constructs. In the second approach, human GFP labeled endothelial networks in the explanted constructs were examined for the presence of auto-fluorescent red blood cells by confocal microscopy.

### 2.11. Quantitative real-time PCR

RT-qPCR was performed to determine the expression of the different myosin heavy chain isoforms (*MYH1*, *MYH3*, *MYH8*) and myogenin (*MyoG*) in the 3 types of human BAMs to reflect the developmental state of the myotubes in the tissue-engineered constructs. To normalize for the amount of cells, 3 reference genes were used: *GAPDH*, *HSP90AB1* and *RPL13A*. RT-qPCR was performed as described previously [31]. Briefly, BAMs were washed with PBS and lysed by sonication. After centrifugation (5 min, 2600 g), high quality total RNA was isolated from supernatant using the PureLink RNA Mini Kit (Ambion #12 183 018A) as evaluated by A260/A280. 2  $\mu\text{g}$  of isolated RNA was reverse transcribed with the

**Table 1.** List of primers used for RT-qPCR.

Gene	Orientation	Primer sequence (5'—3')	Amplicon size (bp)
<i>MYH1</i>	Forward	GGG AGA CCT AAA ATT GGC TCA A	106
	Reverse	TTG CAG ACC GCT CAT TTC AAA	
<i>MYH3</i>	Forward	CTT GTG GGC GGA GGT CTG G	119
	Reverse	AGC TAT GCC GAA CAC TTC CAT	
<i>MYH8</i>	Forward	ACA TTA CTG GCT GGC TGG AC	143
	Reverse	ACC TTT CTT CGC GCT GCT AT	
<i>MyoG</i>	Forward	GTG TGT AAG AGG AAG TCG GTG TC	90
	Reverse	GAA GGC CTC ATT CAC CTT CTT	
<i>GAPDH</i>	Forward	TCA AGA AGG TGG TGA AGC AGG	168
	Reverse	ACC AGG AAA TGA GCT TGA CAA A	
<i>HSP90AB1</i>	Forward	AGA AAT TGC CCA ACT CAT GTC C	75
	Reverse	ATC AAC TCC CGA AGG AAA ATC TC	
<i>RPL13A</i>	Forward	CCT GGA GGA GAA GAG GAA AGA GA	126
	Reverse	TTG AGG ACC TCT GTG TAT TTG TCA A	

qScript cDNA SuperMix (Quantabio #95 048-100). PCR was performed with GeneAmp® PCR System 9700 (Applied Biosystems). Gene-specific primers (table 1) were designed using NCBI/Primer-Blast and Primer3plus. Primer efficiency was determined by serial dilution of cDNA during RT-qPCR and verified to be >90%. RT-qPCR was performed with the LightCycler® 480 Instrument (Roche) using Perfecta Sybr Green Supermix (Quantabio #95 054-500). All samples, 10  $\mu$ l reaction volume, were run in technical duplicates. 40 cycles were run with a DNA dissociation step (95 °C, 15 s), a primer annealing step and an amplification step (60 °C, 45 s). Melting curve analysis was performed to verify the amplification product. Relative mRNA expression was statistically analyzed with relative expression software tool (REST 2009, Qiagen). The REST software calculates whether gene expression is significantly different between the sample and control group using bootstrap randomization [32].

### 2.12. Statistics

Number of replicates refers to number of analyzed images for microscopic analyses or to number of BAMs for thickness analyses. D'Agostino & Pearson normality test and Bartlett's test were used to verify normality of the data and equality of variances, respectively. Normally distributed data with equal variances were analyzed by an unpaired student t-test when two groups were compared. For comparing several normally distributed groups, a one-way ANOVA was used with a Bonferroni multiple comparison post test. For groups that were not normally distributed and/or had unequal variances, a non-parametric Mann-Whitney test was used for comparison between two groups while Kruskal-Wallis test followed by a Dunn's post test was performed for multiple comparisons. All values of analyzed images and relative expression data were displayed in Whisker boxplots and thickness analyses as mean  $\pm$  standard deviation. \*  $p < 0.05$ , \*\*  $p < 0.01$ , \*\*\*  $p < 0.001$ .

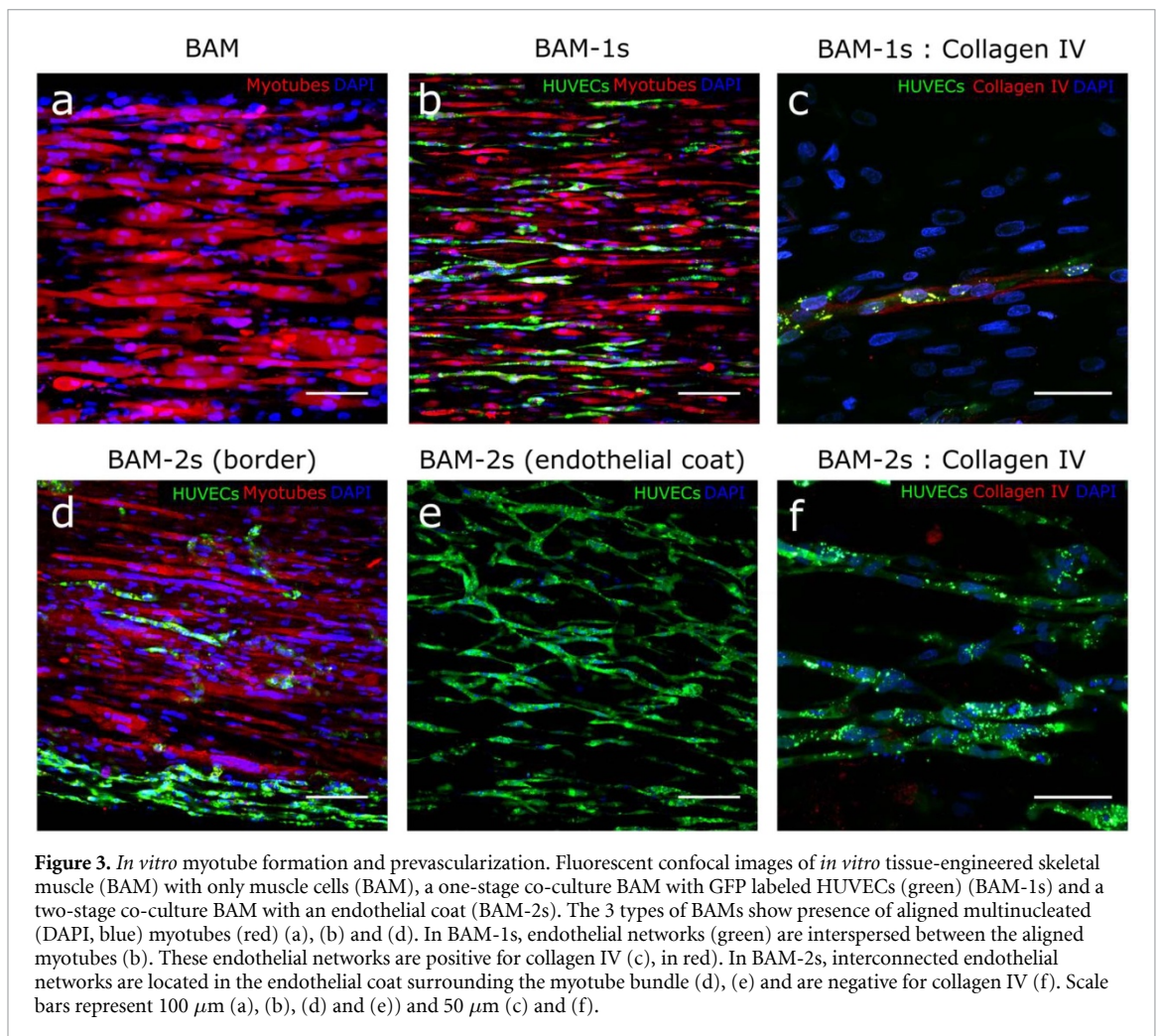
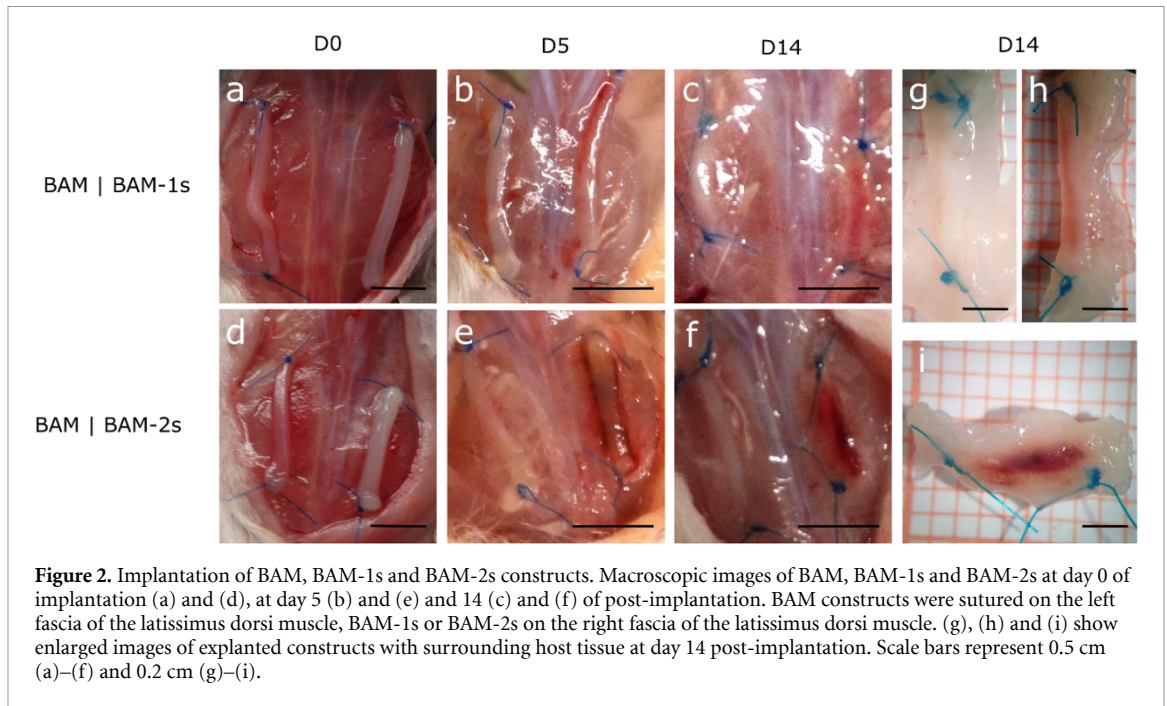
## 3. Results

### 3.1. In vitro BAM formation

First, cells isolated from a human muscle biopsy were expanded and characterized. This muscle cell population, previously described in [31] contained  $82 \pm 5\%$  desmin-positive myoblasts ( $n = 6$ ) at 12 doublings. Myoblasts had a fusion index of  $80 \pm 15\%$  ( $n = 6$ ) as determined by tropomyosin staining, forming myotubes with  $10 \pm 4$  nuclei per myotube (figure S1 (available online at [stacks.iop.org/BF/V/A/mmedia](https://stacks.iop.org/BF/V/A/mmedia))). To make bio-artificial muscle with only muscle cells (BAM),  $2 \times 10^6$  muscle cells were mixed in a fibrin extracellular matrix ( $1 \text{ mg ml}^{-1}$ ) and cultured in skeletal muscle growth medium (SkGM) for 2 d, followed by skeletal muscle differentiation medium (SkFM) for 12 d. The cell-fibrin hydrogel mix contracted around 2 attachment points and formed a 2 cm long muscle bundle (schematic representation in figure 1, macroscopic image in figures 2(a) and (d)), containing aligned multinucleated myotubes (figure 3(a)) with a thickness of  $1.25 \pm 0.2 \text{ mm}$  ( $n = 21$ ).

### 3.2. In vitro myotube formation in prevascularized BAMs

Two different prevascularization strategies of BAMs were evaluated. The first approach was previously evaluated *in vitro* and described in [10]. This co-culture strategy, here termed the 1-stage prevascularization (or BAM-1s) was made by co-culturing muscle cells with endothelial cells (HUVECs) in a 70:30 ratio and a total number of  $2 \times 10^6$  cells in fibrin hydrogel (schematic representation in figure 1, macroscopic image in figure 2(a) right side). As we described previously, culturing HUVECs in skeletal muscle media results in poor HUVEC survival, therefore we cultured BAM-1s in EGM-2, an optimized medium for endothelial cells [10]. After 1 week in culture, the cell—fibrin hydrogel contracted to a muscle bundle with interspersed endothelial network



and a total thickness of  $1.34 \pm 0.15$  mm ( $n = 16$ ) (figure 2(a) right side). No significant difference in BAM-1s thickness was present in comparison to

BAM. However, as reported before [10], myotube formation in BAM-1s is compromised in the EGM medium resulting in decreased myotube diameter,

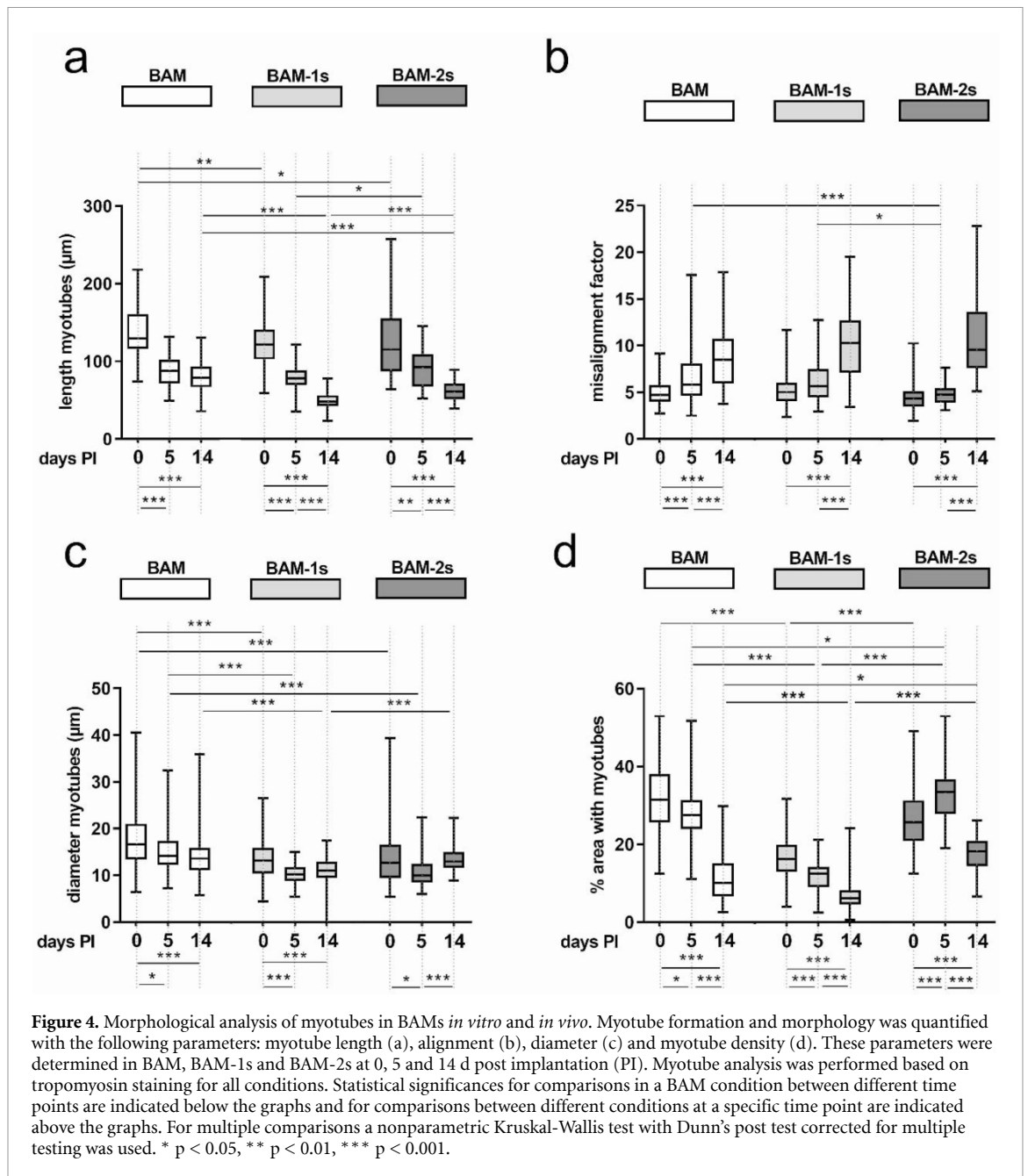
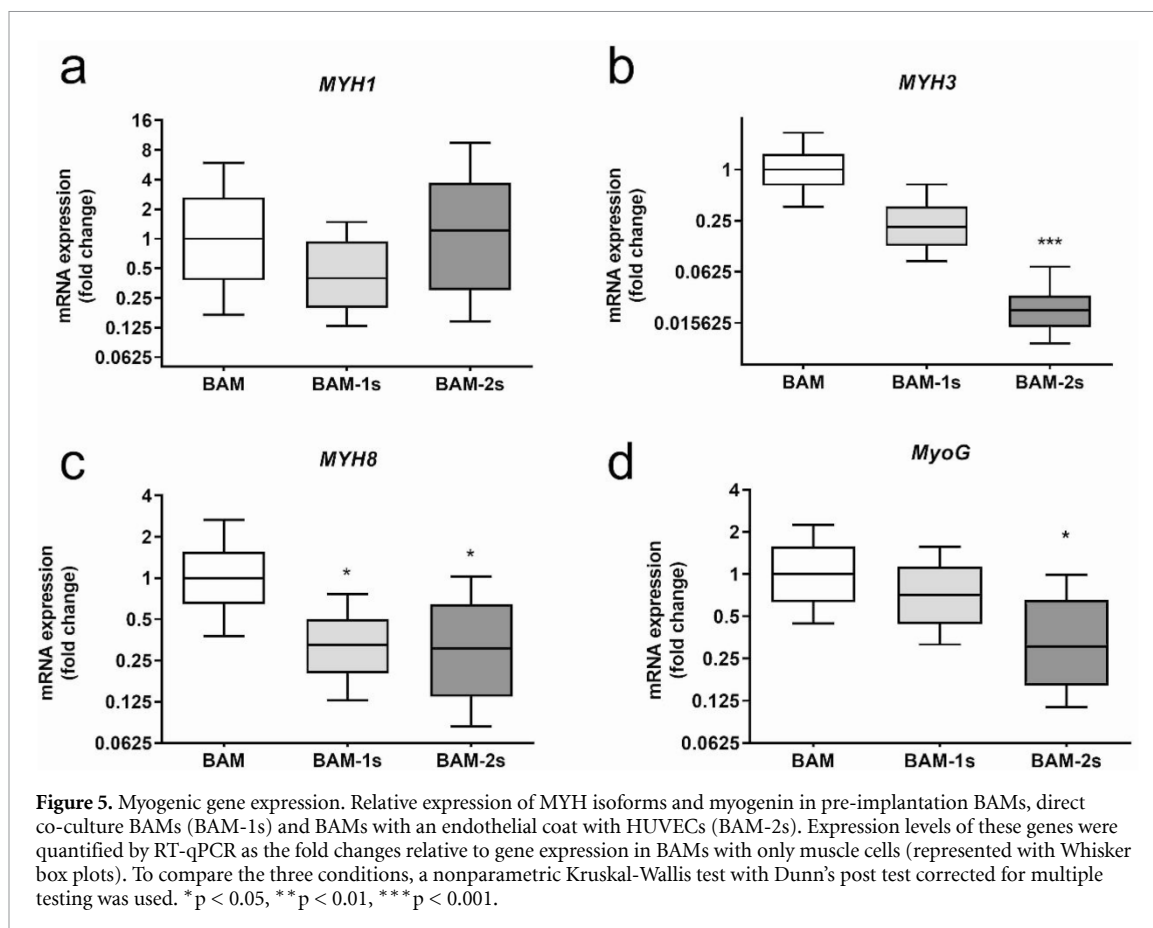


**Figure 4.** Morphological analysis of myotubes in BAMs *in vitro* and *in vivo*. Myotube formation and morphology was quantified with the following parameters: myotube length (a), alignment (b), diameter (c) and myotube density (d). These parameters were determined in BAM, BAM-1s and BAM-2s at 0, 5 and 14 d post implantation (PI). Myotube analysis was performed based on tropomyosin staining for all conditions. Statistical significances for comparisons in a BAM condition between different time points are indicated below the graphs and for comparisons between different conditions at a specific time point are indicated above the graphs. For multiple comparisons a nonparametric Kruskal-Wallis test with Dunn's post test corrected for multiple testing was used. \*  $p < 0.05$ , \*\*  $p < 0.01$ , \*\*\*  $p < 0.001$ .

length and density compared to BAM (compare figure 3(a) with 3(b) and figures 4(a), (c) and (d). No difference in myotube alignment was observed (figure 4(b)). RT-qPCR analysis of pre-implantation BAM, BAM-1s and BAM-2s for myosin heavy chain (MYH) isoform expression showed a presence of less mature myotubes (figure 5) in BAM-1s compared to BAM reflected by a 2.5 and 4.7-fold lower expression level of respectively the adult isoform MYH1 and the perinatal isoform MYH8. Also, a respectively 3-fold and 1.4-fold lower expression level was observed for the embryonic isoform MYH3 and myogenin, indicating a lower myogenic differentiation in BAM-1s. Earlier reports on the *in vitro* evaluation of this co-culture BAM-1s also described a decrease in myotube diameter and density compared to BAM [10].

To circumvent this compromised myotube formation, we also explored a two-stage prevascularization approach (BAM-2s). First,  $2 \times 10^6$  muscle cells were mixed with a fibrin hydrogel ( $1 \text{ mg ml}^{-1}$ ) to engineer a one-week old BAM as described before [10]. Then, we embedded the BAM in a fibrin hydrogel containing  $2 \times 10^6$  HUVEC cells, further referred to as the endothelial coat. In each tissue-engineering stage, a  $2 \times 10^6 \text{ cell ml}^{-1}$  ratio was used, as was done with BAM and BAM-1s. This construct was cultured for another week in EGM-2 to stimulate endothelial network formation (schematic representation in figure 1, macroscopic image in figure 2(d) right side). Endothelial cells in this coat layer spontaneously formed endothelial networks, and this layer was  $117 \pm 12 \mu\text{m}$  thick ( $n = 6$ ) one week after casting (figure 3(e)). The



advantage of this procedure is that differentiation of each cell type occurred in its own specialized medium, resulting in better survival and morphology of each cell type. The resulting BAM-2s was  $1.5 \pm 0.15$  mm thick ( $n = 16$ , figure 2(d)), which was significantly thicker than BAM and BAM-1s. After 14 d in culture, we visualized myotube formation using confocal microscopy (figure 3(d)). Myotube density was significantly higher in BAM-2s compared to BAM-1s and similar to BAM (figure 4(d)). Myotube length and diameter *in vitro* was highest in BAM (figures 4(a) and (c)). No differences were observed for myotube alignment between the 3 different BAM types (figure 4(b)). Regarding MYH isoform expression in BAM-2s, no difference with BAM was observed for *MYH1*. A lower expression of *MYH3*, *MYH8* and myogenin was observed, respectively 45, 3.2 and 3.3-fold lower than in myotubes in BAM (figure 5). There were no significant differences in *MYH* or myogenin expression in BAM-2s versus BAM-1s (figure 5).

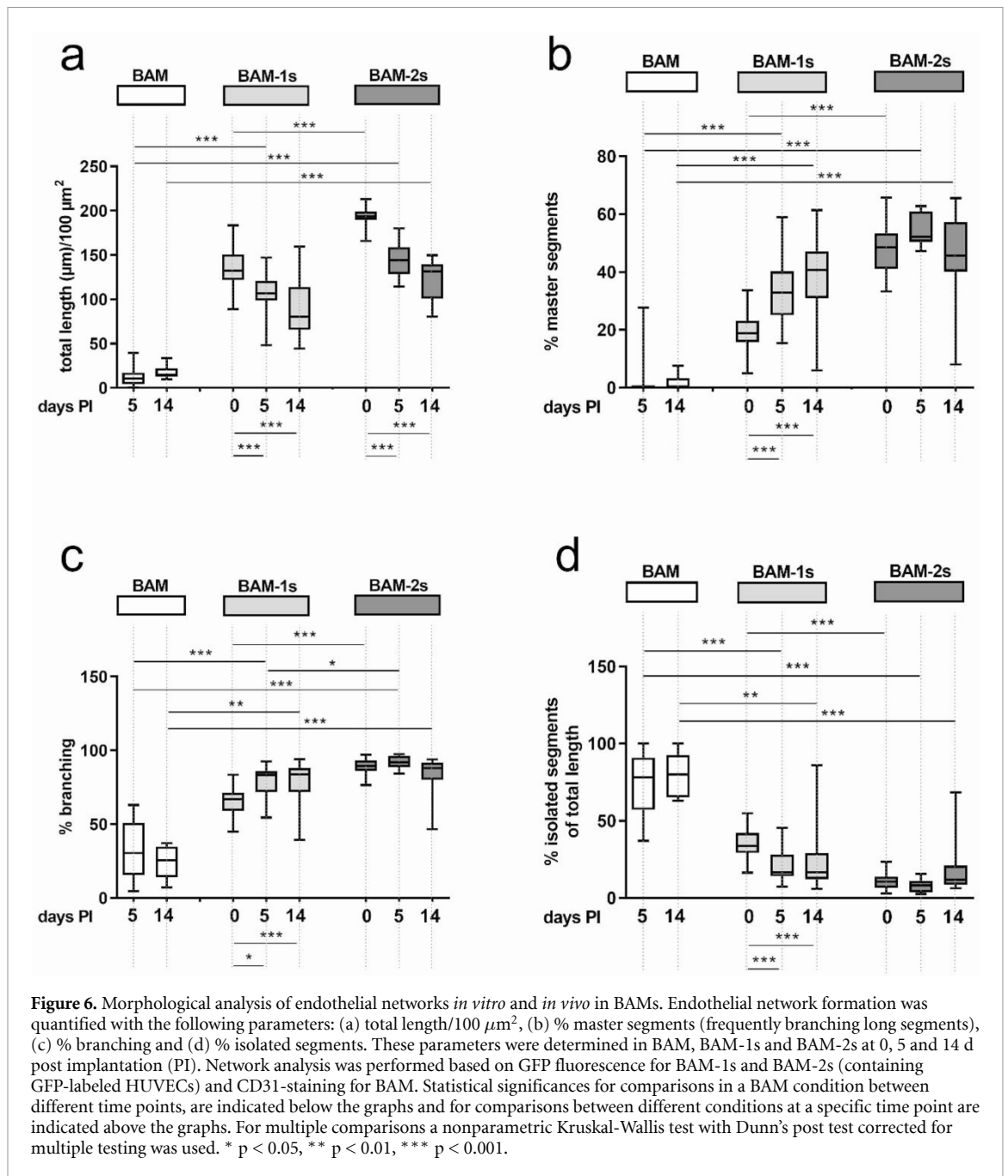
### 3.3. In vitro endothelial network formation in BAM-1s and BAM-2s

Endothelial networks were formed through self-assembly and self-organization in BAM-1s and BAM-2s fibrin constructs (figures 3(b), (d) and (e)). In BAM-1s, endothelial networks were interspersed between aligned myotubes. In BAM-2s,

the endothelial networks (figure 3(e)) penetrated the myotube bundle occasionally in the transition area between the BAM and the endothelial coat (figure 3(d)). When comparing endothelial networks in BAM-1s and BAM-2s, a higher network complexity could be observed in BAM-2s (figures 3(b), (e) and 6). For all measured parameters, BAM-2s outperformed BAM-1s (figure 6). This means that in BAM-2s, the endothelial networks were longer, more branched with less isolated segments not participating in a network compared to BAM-1s. Although the endothelial network characteristics were better in BAM-2s than BAM-1s, they were negative for collagen IV, a basement membrane protein important in vascular maturity and stabilization [33] (figure 3(f)). Networks in BAM-1s were positive for collagen IV (figure 3(c)) but they regressed after one week *in vitro*, a clear indication of the poor stability of the network (figure S2).

### 3.4. In vivo implantation and explantation

Next, we evaluated whether different strategies of pre-vascularization affected the constructs in terms of (i) myotube survival, (ii) myotube maturation and (iii) functionality of the endothelial networks *in vivo*. Therefore, we implanted the three BAM types on the fascia of the *latissimus dorsi* muscle on the back of NOD/SCID mice. The prevascularized constructs (BAM-1s and BAM-2s) were implanted on the right



fascia of the *latissimus dorsi* muscle, while BAMs (without prevascular networks) were implanted on the left fascia of the *latissimus dorsi* (figures 2(a) and (d)) as a reference. Both on day 5 and day 14 post implantation (PI), differences in vascularization between constructs could be observed macroscopically (figures 2(b) and (e), (c) and (f), (h) and (i)). While the appearance of the muscle cell only BAM construct did not change (white), BAM-1s and BAM-2s were red, pointing to the presence of blood (figures 2(b), (c) and (e), (f); right side). In contrast to day 5, the different types of BAM were integrated with host tissue at day 14. Therefore, BAM constructs were explanted together with surrounding host tissue at day 14. To visualize myotube characteristics throughout the whole construct at day 14

PI, the tissue was cut into 200  $\mu\text{m}$  sections with a vibratome.

### 3.5. In vivo myotube maintenance

Myotube survival and maturation *in vivo* were evaluated morphologically at 5 and 14 d after implantation. Myotubes were still present at day 14 of implantation in all conditions (figure 7). However, compared to pre-implantation, a reduction in myotube length in all conditions was shown at day 5 which was even more prominent at day 14 (figure 4(a)). At this time point, myotube length was decreased by 40% (BAM), 61% (BAM-1s) and 47% (BAM-2s). Similarly, myotube alignment decreased over 14 d, depicted in figure 4(b) as an increase in misalignment. On the other hand, there was an overall decrease from

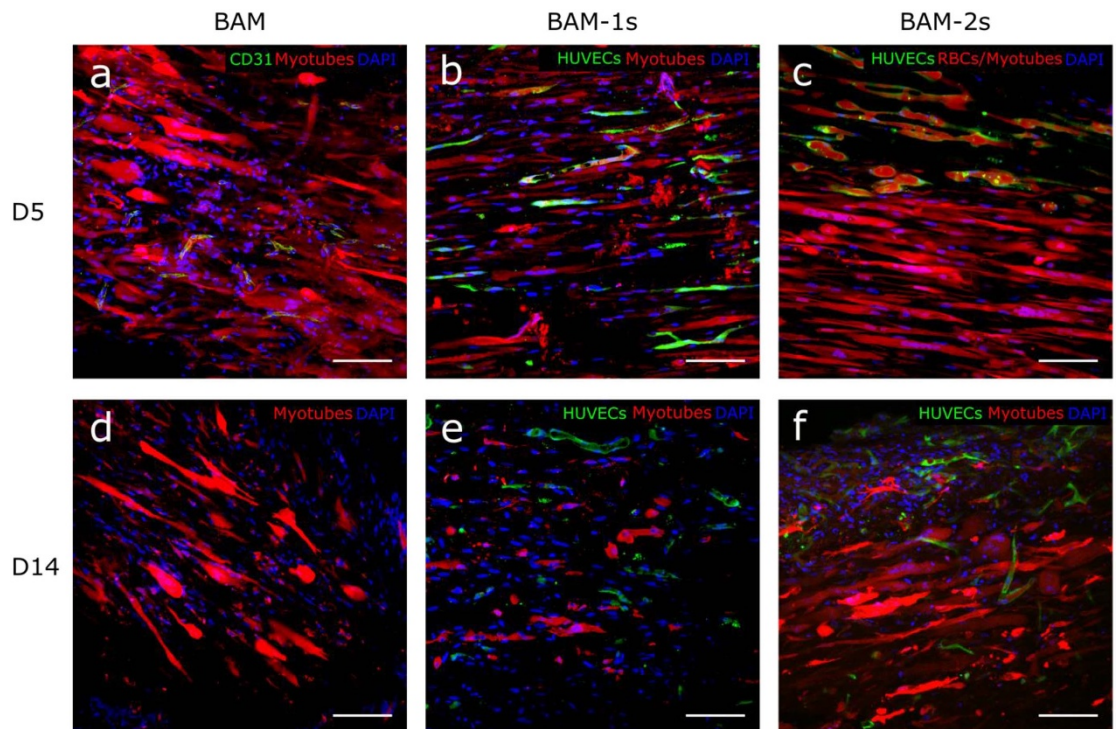


**Figure 7.** Confocal images of myotube and endothelial network in BAMs 5 and 14 d post-implantation. Fluorescent confocal images of muscle cell only BAMs explanted after 5 (a) or 14 d (d) *in vivo* showing myotubes (red), nuclei (DAPI, blue) and endothelial cells (CD31, green). Images with the same setup are shown for BAM-1s explanted after 5 (b) or 14 (e) days and BAM-2s explanted after 5 (c) or 14 (f) days. For BAM-1s and BAM-2s, endothelial cells are labeled with GFP. Scale bars represent 100  $\mu\text{m}$ .

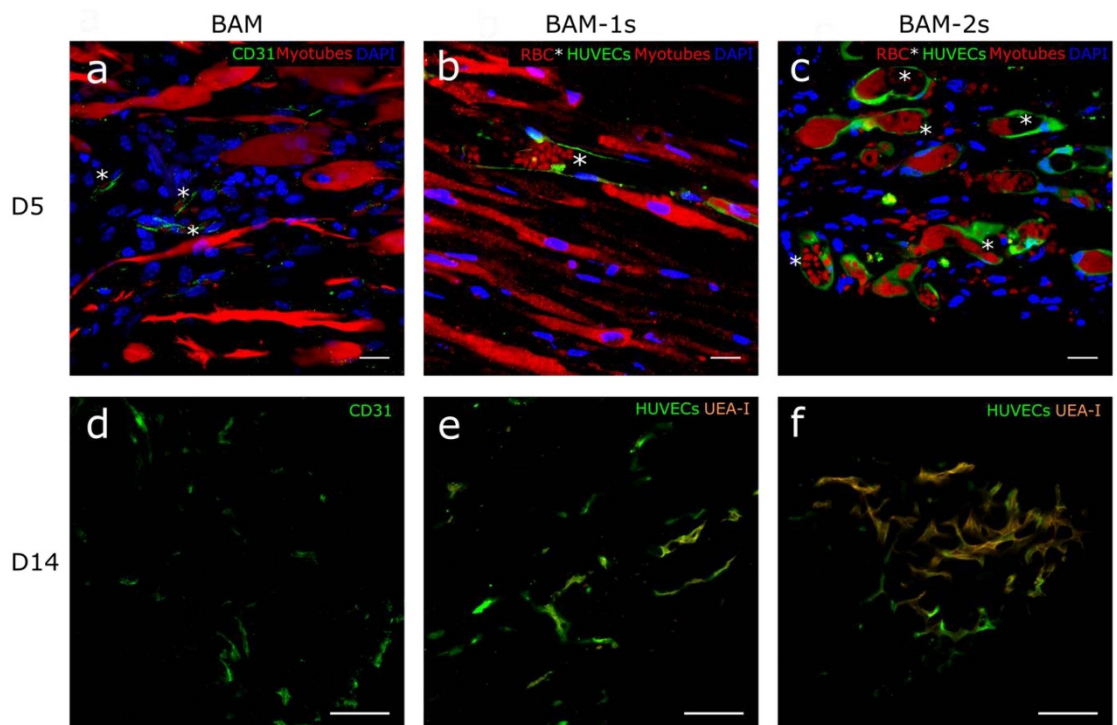


**Figure 8.** *In vivo* perfusion of prevascularized endothelial networks at 5 and 14 d post-implantation. Fluorescent confocal images of implanted BAM at day 5 and day 14 with only muscle cells (BAM) and CD 31 positive capillaries (green) (a) and (d), of a one-stage co-culture BAM with GFP labeled HUVECs (BAM-1s) (green) (b) and (e) and a two-stage co-culture BAM with an endothelial coat containing GFP labeled HUVECs (green) (BAM-2s) (c) and (f). At day 5 post-implantation prevascularized BAMs contain GFP labeled endothelial vessels (green) that are perfused with red blood cells (red dots, asterisks (b) and (c)). At day 14 GFP labeled endothelial vessels (green) are UEA-I positive (orange) (e) and (f), showing perfusion of the newly formed blood vessels due to anastomosis between host vessels and implanted networks. Muscle cell only BAMs contain some CD31 positive capillaries but no perfusion of the construct with UEA-I at day 14 was observed (d). Scale bars represent 20  $\mu\text{m}$  (a)–(c) and 100  $\mu\text{m}$  (d)–(f).

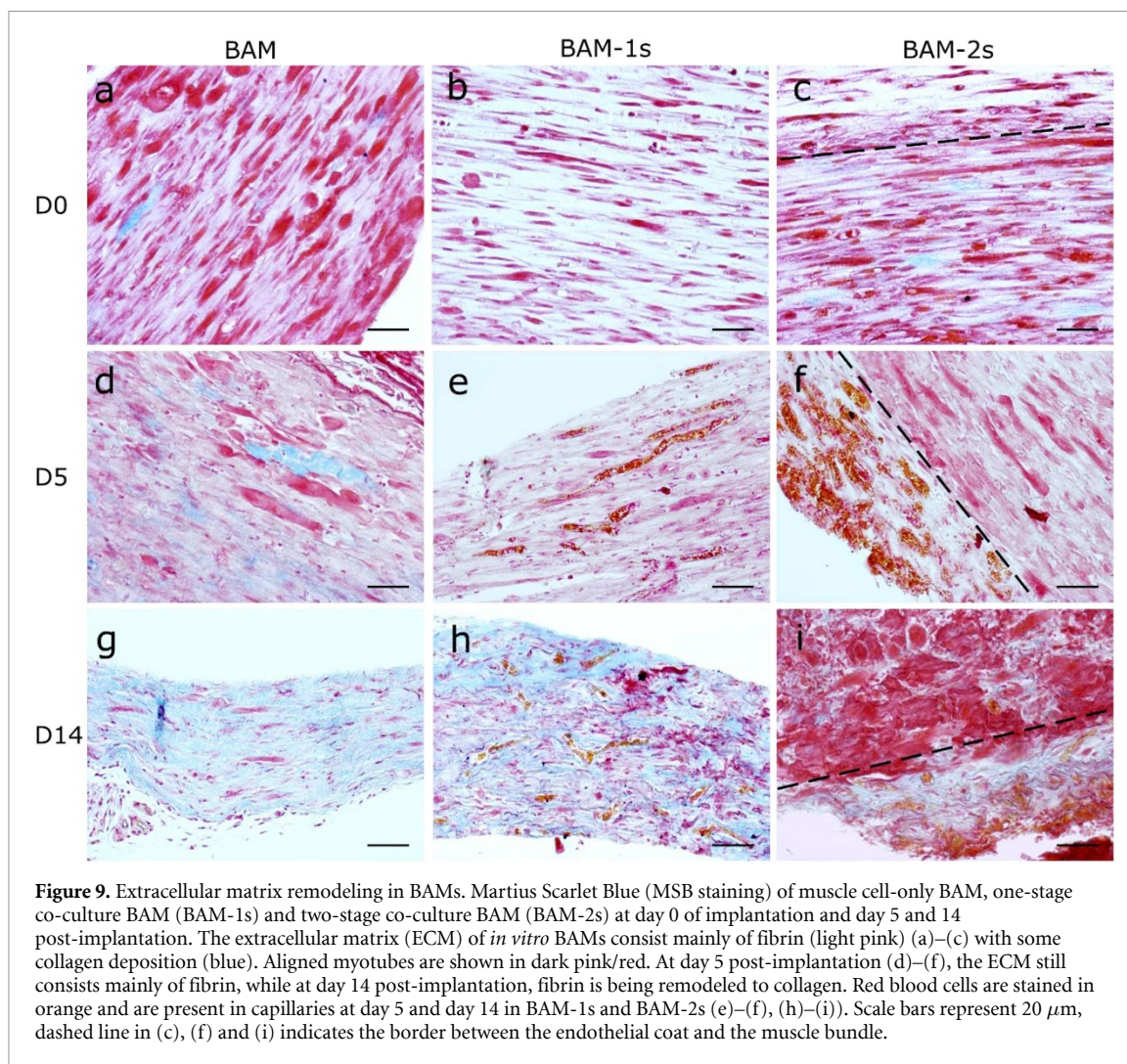


**Figure 9.** Extracellular matrix remodeling in BAMs. Martius Scarlet Blue (MSB staining) of muscle cell-only BAM, one-stage co-culture BAM (BAM-1s) and two-stage co-culture BAM (BAM-2s) at day 0 of implantation and day 5 and 14 post-implantation. The extracellular matrix (ECM) of *in vitro* BAMs consist mainly of fibrin (light pink) (a)–(c) with some collagen deposition (blue). Aligned myotubes are shown in dark pink/red. At day 5 post-implantation (d)–(f), the ECM still consists mainly of fibrin, while at day 14 post-implantation, fibrin is being remodeled to collagen. Red blood cells are stained in orange and are present in capillaries at day 5 and day 14 in BAM-1s and BAM-2s (e)–(f), (h)–(i)). Scale bars represent 20  $\mu\text{m}$ , dashed line in (c), (f) and (i) indicates the border between the endothelial coat and the muscle bundle.

day 0 to day 14 PI in myotube diameter for BAM and BAM-1s conditions, while this was not the case for BAM-2s. Finally, myotube density decreased in all conditions from day 0 to day 14 PI although this effect was least prominent in the BAM-2s condition (67.8% (BAM), 61% (BAM-1s) and 33.4% (BAM-2s), figures 4(d) and 7(d), (e) and (f)).

### 3.6. *In vivo* vascularization and anastomosis

*In vivo* vascularization of BAMs was assessed 5 and 14 d after implantation. GFP labeled endothelial vessels, which originated from the HUVECs, were present in BAM-1s and BAM-2s at day 5 and 14 (figures 6, 7 and 8). Ingrowth of host blood vessels in muscle cell only BAM was visualized by CD31-staining. There was a higher vascular density, determined by total network length per 100  $\mu\text{m}^2$ , in the prevascularized BAMs compared to muscle cell only BAM (figures 6(a) and 7). After 5 d *in vivo*, the location of the endothelial vessels remained similar as to the situation *in vitro* for BAM-1s and BAM-2s: while interspersed between myotubes in BAM-1s, endothelial vessels in BAM-2s surrounded the myotube bundle (figures 7(b) and (c)). However, at

day 14, vascular structures derived from HUVECs were also observed between myotubes in BAM-2s (figure 7(f)). Although there was a general decrease in the vascular density in both prevascularized constructs, pointing to degeneration of part of the network (figure 6(a)), the remaining network was more interconnected (figures 6(c) and (d)). To assess the functionality of the networks, a rhodamin-labelled human EC specific agglutinin (UEA-I) was injected intravenously. Detection of this dye within the BAMs points to a functional network which is anastomosed with the host blood vessels [5]. The latter could also be verified by the presence of red blood cells in the GFP labeled networks. At day 5, in both BAM-1s and BAM-2s, the majority of endothelial vessels (>90%) contained red blood cells, while only sparse presence of UEA-I-positive endothelial networks was observed (figures 8(b) and (c)). This pointed to early anastomosis with little perfusion. At day 14, a part of the GFP-labeled endothelial vessels in BAM-1s and BAM-2s were UEA-I positive (figures 8(e) and (f), S3, supplementary Videos S1 and S2) and contained red blood cells (figures 8(b) and (c), supplementary Video S3), showing functionality of implanted networks.

### 3.7. Extracellular matrix remodeling after implantation

Extracellular matrix (ECM) remodeling *in vivo* was evaluated by Martius Scarlet Blue (MSB) which stains muscle tissue red, fibrin pink/purple, collagen blue and red blood cells orange. The ECM of *in vitro* cultured BAMs mainly consists of fibrin (figures 9(a)–(c)) with limited deposition of collagen. No significant ECM remodeling had occurred by day 5 PI (figures 9(d)–(f)). The presence of myotubes as seen with confocal microscopy (figure 7) was confirmed with MSB staining (figure 9). The presence of blood vessels in BAM-1s and BAM-2s constructs was also confirmed with MSB staining; red blood cells stained in orange were clearly detectable and located within the BAM-1s or surrounding the BAM-2s (figures 9(e), (f), (h) and (i)). After 14 d *in vivo*, fibrin ECM in BAM and BAM-1s was remodeled into a collagen ECM (figures 9(g) and (h)). In BAM-2s, a difference could be observed between the inner part of the construct containing mainly myotubes with traces of fibrin and collagen versus the endothelial coat which showed primarily collagen as ECM (figure 9(i)).

## 4. Discussion

At present, the use of muscle flaps to treat volumetric muscle loss has significant drawbacks [2]. Tissue engineered skeletal muscle holds promise for an alternative treatment. The tissue-engineering approach used in this paper further builds on a muscle tissue engineering approach, called bio-artificial muscle (BAM) containing aligned myotubes [23, 34]. Still, many challenges towards clinical as well as *in vitro* testing applications remain. One of them is the limited size of the constructs, imposed by the limit of passive diffusion of nutrients and gases. Prevascularization is being explored as a method to allow *in vitro* perfusion and to enhance *in vivo* survival and engraftment of tissue-engineered constructs [12, 35, 36]. In this paper, we have evaluated two prevascularization strategies of tissue-engineered bio-artificial muscle (BAM) to tackle the limitation.

The first approach was previously evaluated *in vitro* [10]. In this one-stage prevascularization approach (BAM-1s) a direct co-culture of endothelial cells and muscle cells resulted in aligned multinucleated myotubes with interspersed endothelial networks. The natural hydrogel fibrin was used as a scaffold, because of its pro-angiogenic and stiffness characteristics [37]. As reported before [10] myotube formation was suboptimal in the endothelial growth medium (EGM) in which BAM-1s was cultured when compared to BAMs cultured in skeletal muscle cell-specific media (SkGM/SkFM). The impaired myotube formation in EGM was also described by others [12] but is unavoidable in the one-stage approach since EC survival is severely compromised

in SkGM/SkFM. In this follow-up study, the goal was to test the functionality of the preformed endothelial networks after implantation *in vivo*.

To avoid the reported suboptimal myotube formation in BAM-1s, we established another prevascularization strategy, consisting of two stages, termed BAM-2s. In the first stage, muscle cell-only BAMs were cultured for one week in SkGM/SkFM, allowing for optimal myotube formation. In a second stage, an endothelial cell coat was added in which endothelial networks formed during the second week. Then, the BAM-2s was cultured in EGM, supporting survival and differentiation of the ECs. This two-stage strategy indeed resulted in less compromised myotube formation, while supporting endothelial network formation even stronger than in the one-stage approach. Also these BAM-2s were tested in an *in vivo* setting in this study.

We are aware that there are multiple differences between the one-stage and two-stage prevascularization protocols since both strategies have been optimized separately to produce the best possible co-culture BAM. For example, the prolonged culture time of the muscle cells in the two-stage approach resulted in better myotube formation, as also reported elsewhere [38]. However, applying the same culture time in the one-stage approach was detrimental for the ECs since culturing BAM-1s longer than 1 week resulted in endothelial network degradation (figure 2(s)).

Vascularization is key for muscle development and function. Therefore, we assessed the myogenic gene expression in the three types of BAMs before implantation using quantitative real-time PCR. Myosin heavy chain isoforms reflect the developmental state of muscle fibers [39]. Relative expression levels of MYH1, MYH3, MYH8 and myogenin were analyzed to assess the influence of our vascularization strategy on muscle development. Myogenin expression is indicative for early myogenic differentiation and myofiber formation [31] while MYH3, MYH8 and MYH1 are expressed in embryonic, perinatal and adult stages, respectively. Analysis showed that the significantly higher MYH8, MYH3 and/or myogenin levels indicate a more active myofiber formation in BAM compared to BAM-1s or BAM-2s. This is not surprising given the optimal conditions for myofiber formation provided by the skeletal muscle fusion medium in this condition. No significant difference in adult isoform MYH1 expression was observed between the three conditions pointing out that pre-implantation, the endothelial networks were not able to promote muscle fiber maturation. The BAM-2s approach was explored with the intention to improve myogenesis and/or vasculogenesis compared to the BAM-1s strategy. Although this was successful, the BAM-2s still underperformed compared to the BAM regarding myogenesis, as shown by the image analysis and qPCR data. This can be explained by the need to maintain the BAM-2s in EGM for one

week. Myogenic cell lineages are typically cultured in a high-glucose basal medium with at least 10% FBS while the EGM-2 medium only contains 5% FBS. The negative impact on myogenic cell lineages when defining co-culture media has been described by us and others [10, 12, 40]. Still, the BAM-2s provided the best trade-off between vasculogenesis and myogenesis in a tissue engineered muscle construct.

Characterization of endothelial networks *in vitro* indicated that the most interconnected networks with the highest vascular density were observed in BAM-2s. Indeed, an increased endothelial cell density in the fibrin hydrogel was already described to result in an enhanced number of branches and total vessel length [13], and this is consistent with the high endothelial cell density in the coat of the BAM-2s approach. Also, our previous study showed improved endothelial network formation *in vitro* when a higher density of endothelial cells was used [10]. A well-organized endothelial network *in vitro* is important for the *in vivo* vascularization and tissue integration in the host tissues as shown before [5, 19]. One week after implantation, the extent of vascularization in the co-culture flaps was greater than in the myotube only flaps. Vascularization and efficient perfusion are also challenges in cardiac tissue engineering. Perfusable microvascular constructs containing patterned microchannels with endothelial cells integrated with the coronary vasculature of infarcted rat hearts to a greater degree than non-perfusible constructs at 5 d post-implantation [41].

Besides analysis of morphological parameters, collagen IV deposition was assessed. Collagen IV is the main component of the vascular basement membrane matrix. Basement membrane matrix assembly is a critical step in vessel maturation and vessel stability as observed in *in vitro* and developmental studies [33, 42–44]. Endothelial networks in BAM-1s were surrounded by a thin layer that contained collagen IV, suggesting the presence of a basement membrane, in contrast to endothelial networks in BAM-2s. In BAM-1s, endothelial cells were mixed with muscle cells containing both myoblasts and fibroblasts [10], in contrast to BAM-2s where only endothelial cells were present in the coat region. Several groups have successfully shown that addition of mesenchymal-derived cells, such as fibroblasts, pericytes and/or smooth muscle cells improved endothelial network maturation and *in vitro/in vivo* network stabilization in tissue engineered constructs [45–49]. These cells are able to differentiate into supportive mural cells around newly formed endothelial networks in co-culture settings with endothelial cells [47, 50, 51]. Pericytes for example are known for their role in stimulating basement membrane matrix deposition by endothelial cells [33]. Optimizing fibroblast—endothelial cell ratios and/or evaluation of other mesenchymal-derived cells as mural cells may still improve prevascularization outcome in the two-stage

approach. In this study we have used HUVECs as endothelial cell source. HUVECs are easy to isolate, abundant and well characterized. Furthermore, they are capable of endothelial network formation *in vitro* [5, 10, 12]. Other examples of endothelial cell sources able to form endothelial networks are microvascular endothelial cells [52], embryonic heart endothelial cells [53], pluripotent cell derived endothelial cells [54] and blood outgrowth endothelial cells [55] and are worthwhile for further investigation in prevascularization strategies.

To evaluate whether prevascularization improves *in vivo* myotube survival and tissue perfusion we implanted BAMs with and without endothelial networks on the fascia of the *latissimus dorsi* muscle of NOD/SCID mice for 5 or 14 d. In all conditions, myotubes were still observed at day 14 of implantation in the construct. However, myotube length, density and alignment decreased in all conditions *in vivo*. Myotube length was decreased by 40% (BAM), 61% (BAM-1s) and 47% (BAM-2s) over 14 d while myotube density was decreased by 67.8% (BAM), 61% (BAM-1s) and 33.4% (BAM-2s). This deterioration in myotube characteristics over time could be caused by the initial lack of perfusion. The detrimental effects of this initial hypoxia state on the myotubes are not completely counteracted, as also reported elsewhere [56]. In addition, the supply of nutrients and oxygen in the first days *in vivo* was limited compared to the *in vitro* situation where constructs were completely submerged in a nutrient-rich medium. Finally, the decrease may also be explained by the occurrence of xenogeneic rejection. Although NOD/SCID mice lack functional T and B cells, have impaired macrophage function and lack the complement system [57], a low level of natural killer (NK) cell activity remains present [58–60]. Macrophage, neutrophil and mast cell invasion may also result in rejection, as seen with implantation of human mesenchymal stem cells on poly( $\epsilon$ -caprolactone) in a NOD/SCID model [60]. Immunodeficient animal models are also deprived of pro-regenerative effects of the immune response during skeletal muscle repair [61–63]. Inflammatory cells, such as macrophages and neutrophils, are recruited and start producing growth factors and cytokines important for satellite cell activation, proliferation and differentiation and capillary ingrowth to injured muscle [2]. For clinical application, use of human autologous muscle and endothelial cells would eliminate xenogeneic responses. In our study, the overall decrease in myotube density was least present for the BAM-2s which we hypothesize to be due to (i) the improved myotube characteristics before implantation compared to the BAM-1s and (ii) the pre-vascularization which was absent in the BAM. An implantation time exceeding 14 d may even improve myotube maturation as reported previously [64]. As the ultimate aim was to develop a muscle

tissue engineering strategy with a prevascularization approach balancing between optimal vasculogenesis and myogenesis, the comparison between BAM-1s vs BAM-2s is crucial. We can conclude that for three out of four measured parameters for myotube characteristics, the two-stage prevascularization approach outperformed the one-stage approach.

Next to examining the effects of prevascularization on myotube maintenance *in vivo*, we also evaluated the effect on *in vivo* vascularization. Prevascularized BAMs showed a significantly higher vascular density *in vivo* compared to BAMs with only muscle cells, as reported previously by others in tissue-engineered constructs [12, 19]. In this study, already at day 5 of implantation anastomosis of the implanted networks with host vessels was observed by the presence of red blood cells in the human endothelial networks. Anastomosis was further confirmed by perfusion of a fluorescent dye injected in the tail vein, which colocalized with the transplanted endothelial cells. Similar to our findings, evidence of anastomosis of endothelial networks in a fibrin gel (without muscle cells) at day 5 PI was found [13]. This anastomosis speed may not be sufficient for oxygen-sensitive tissues such as cardiomyocytes causing ischemia that leads to cell death [65]. Improving the structure and maturation of *in vitro* networks and optimizing the mesenchymal-derived cell/endothelial cell ratio as proposed before [19, 35, 47, 49], addition of exogenous growth factors (e.g. VEGF, FGF and PDGF) to promote *in vivo* vascularization [66] and optimizing fibrin concentration, type and ultrastructure [37, 67] may further reduce anastomosis time and increase vascularization. Despite anastomosis of HUVEC endothelial vessels, shown by red blood cell presence, no perfusion of intravenously injected agglutinin was observed at day 5, suggesting a restricted perfusion. It has been observed with laser speckle imaging that thrombi occurred early after anastomosis of implanted endothelial vessels with host vessels [68]. By day 7 however, functional perfused vessels were reported [68]. In our experiments, onset of full perfusion as demonstrated with fluorescent agglutinin occurred between day 5 and 14 after implantation and showed functionality of the endothelial networks. No differences were found in endothelial network parameters between the one-stage and the two-stage approach constructs.

Fibrin degradation is controlled *in vitro* by modulating the fibrinolysis through fibrinolysis inhibitors. However, *in vivo* fibrinolysis occurs, which results in the rapid degradation of fibrin ECM. Nevertheless, fibrin BAMs maintained structural integrity over 14 d and fibrin ECM was remodeled to collagen as shown by MSB staining in constructs explanted after 14 d. This is in line with previous *in vivo* studies in which fibrin degradation was observed over two weeks in acellular fibrin clots [69] and collagen deposition was shown in tissue engineered skeletal muscle with

a fibrin ECM [64]. Recent work from our group showed that replacement of the degrading fibrin ECM through deposition of autologous collagen enabled the maintenance of the BAM without fibrinolysis inhibition, while increasing the visco-elastic properties of the BAMs [70]. This ECM remodeling can be attributed primarily to fibroblasts that make up 30% of the cell population in the primary human skeletal muscle cells used for making the BAMs. Furthermore, since electrical stimulation has been demonstrated to increase collagen deposition as well, maturing myotubes may also contribute to collagen deposition [71]. The same can be said about ECs which have been shown to locally degrade or deposit matrix proteins upon sprouting [72]. The differences in ECM we observed between the inner myotube part versus the outer endothelial coat of the BAM-2s may be explained by the presence of the vasculature. Taken together, many cell types may contribute to collagen deposition and the results obtained in this work are a combined effect of the presence of fibroblasts and the increased vascularization and myogenesis in and around the implants. ECM remodeling should be controlled, since too extensive collagen deposition might result in fibrotic scarring. This would ultimately interfere with the engraftment and graft function. In this context, the elimination of an inflammatory trigger and resolution of inflammation are important for preventing fibrosis [73]. Furthermore, characterizing the presence of invading immune cells could help understand the evolution of ECM remodeling and engraftment [74, 75]. From our results, no sign of fibrotic tissue was observed around implanted BAMs on histological sections at day 14. Together with the high vascular density and perfusion at day 14 this proves successful engraftment of BAM-1s and BAM-2s as opposed to the muscle cell only BAM, which was not perfused.

In conclusion, we tested two prevascularization strategies of bio-artificial skeletal muscle and evaluated construct survival and engraftment in the host tissue after implantation *in vivo*. The two-stage prevascularization approach resulted in an endothelial network that became functional *in vivo* and supported best myotube survival. Although further improvements can still be done, this strategy opens perspectives for engineering larger skeletal muscle constructs.

## Acknowledgments

The authors are grateful to Stephanie De Vleeschauwer, Erna Dewil and Marleen Lox, Aernout Luttun, Sander Craps, Greetje Vande Velde, Veerle Baekelandt and Joris Van Asselberghs for technical assistance, Rik Gijsbers for miRFP670 cDNA-containing HIV1-derived retroviral vector, Evie Vereecke for human muscle samples, Laurens Willaert and Rune Peyskens for myotube

morphological analysis and Sigrid Vanryckeghem for administrative support. This work was funded by Fonds Wetenschappelijk Onderzoek—Vlaanderen (1.5.298.17 N and mandate to Lisanne Terrie); and AFM-Telethon trampoline grant (19802).

### Conflict of Interest

The authors confirm that there are no known conflicts of interest associated with this publication and there has been no significant financial support for this work that could have influenced its outcome.

### Data availability

The raw data required to reproduce these findings are available to download from <https://data.mendeley.com/datasets/6p47mbpr9f/draft?a=80a2562-a984-4dad-8adb-6bd3060ecac5> and <https://data.mendeley.com/datasets/8gkvvy8j9h/draft?a=1194a3ca-b02e-4627-b1a5-5283b8698986>. The processed data required to reproduce these findings are available to download from <https://data.mendeley.com/datasets/595jwcnkm/draft?a=8ff32c59-4c2f-4312-8c91-18c654ed6a6f>.

### Author contributions

DG and LTh contributed to conception and designed the project. DG performed *in vitro* experiments. DG, KM, LH, LTe, JD were responsible for *in vivo* experiments. DG, LD, LTe performed data collection. DG, Lte, MG and GC performed data analysis and GC performed customized software development. DG and MG performed interpretation and statistical analysis. DG and LTe wrote the manuscript with input from all authors. LTh supervised the project. All authors read and approved the manuscript.

### ORCID iD

L Thorrez  <https://orcid.org/0000-0002-5896-6823>

### References

Q1

- [1] Musarò A 2014 The basis of muscle regeneration *Adv. Biol.* **2014** 1–16
- [2] Järvinen T A, Järvinen T L, Kääriäinen M, Kalimo H and Järvinen M 2005 Muscle injuries: biology and treatment *Am. J. Sports Med.* **33** 745–64
- [3] Lee K T and Mun G H 2014 A systematic review of functional donor-site morbidity after latissimus dorsi muscle transfer *Plast. Reconstr. Surg.* **134** 303–14
- [4] Cittadella Vigodarzere G and Mantero S 2014 Skeletal muscle tissue engineering: strategies for volumetric constructs *Front Physiol.* **5** 362
- [5] Shandalov Y, Egozi D, Koffler J, Dado-Rosenfeld D, Ben-Shimol D, Freiman A, Shor E, Kabala A and Levenberg S 2014 An engineered muscle flap for reconstruction of large soft tissue defects *Proc. Natl. Acad. Sci. USA* **111** 6010–5
- [6] Thorrez L, Shansky J, Wang L, Fast L, VandenDriessche T, Chuah M, Mooney D and Vandenburg H 2008 Growth, differentiation, transplantation and survival of human skeletal myofibers on biodegradable scaffolds *Biomaterials* **29** 75–84
- [7] Folkman J and Hochberg M 1973 Self-regulation of growth in three dimensions *J. Exp. Med.* **138** 745–53
- [8] Orr A W 2003 Thrombospondin signaling through the calreticulin/LDL receptor-related protein co-complex stimulates random and directed cell migration *J. Cell. Sci.* **116** 2917–27
- [9] Cerino G, Gaudiello E, Grussenmeyer T, Melly L, Massai D, Banfi A, Martin I, Eckstein F, Grapow M and Marsano A 2016 Three dimensional multi-cellular muscle-like tissue engineering in perfusion-based bioreactors *Biotechnol. Bioeng.* **113** 226–36
- [10] Gholobova D, Decroix L, Van Mulyder V, Desender L, Gerard M, Carpentier G, Vandenburg H and Thorrez L 2015 Endothelial network formation within human tissue-engineered skeletal muscle *Tissue Eng. Part A* **21** 2548–58
- [11] Laschke M W and Menger M D 2015 Prevascularization in tissue engineering: current concepts and future directions *Biotechnol. Adv.* **34** 112–21
- [12] Levenberg S et al 2005 Engineering vascularized skeletal muscle tissue *Nat. Biotechnol.* **23** 879–84
- [13] Chen X, Aledia A S, Ghajar C M, Griffith C K, Putnam A J, Hughes C C W and George S C 2009 Prevascularization of a fibrin-based tissue construct accelerates the formation of functional anastomosis with host vasculature *Tissue Eng. Part A* **15** 1363–71
- [14] Abou-Khalil R, Mounier R and Chazaud B 2010 Regulation of myogenic stem cell behaviour by vessel cells: the ‘ménage à trois’ of satellite cells, periendothelial cells and endothelial cells *Cell Cycle* **9** 892–6
- [15] Christov C et al 2007 Muscle satellite cells and endothelial cells: close neighbors and privileged partners *Mol. Biol. Cell* **18** 1397–409
- [16] Post M J, Rahimi N and Caolo V 2013 Update on vascularization in tissue engineering *Regen. Med.* **8** 759–70
- [17] Hanjaya-Putra D, Shen Y-I, Wilson A, Fox-Talbot K, Khetan S, Burdick J A, Steenbergen C and Gerecht S 2013 Integration and Regression Of Implanted Engineered Human Vascular Networks During Deep Wound Healing *Stem. Cells Transl. Med.* **2** 297–306
- [18] Bach A D, Arkudas A, Tjiawi J, Polykandriotis E, Kneser U, Horch R E and Beier J P 2006 A new approach to tissue engineering of vascularized skeletal muscle *J. Cell Mol. Med.* **10** 716–26
- [19] Koffler J, Kaufman-Francis K, Yulia S, Dana E, Daria A P, Landesberg A and Levenberg S 2011 Improved vascular organization enhances functional integration of engineered skeletal muscle grafts *Proc. Natl. Acad. Sci. USA* **108** 14789–94
- [20] Higgins S P, Solan A K and Niklason L E 2003 Effects of polyglycolic acid on porcine smooth muscle cell growth and differentiation *J. Biomed. Mater. Res.* **67A** 295–302
- [21] Freiman A, Shandalov Y, Rosenfeld D, Shor E, Ben-David D, Meretzki S, Levenberg S and Egozi D 2018 Engineering vascularized flaps using adipose-derived microvascular endothelial cells and mesenchymal stem cells *J. Tissue Eng. Regen. Med.* **12** e130–41
- [22] Vandenburg H, Shansky J, Del Tatto M and Chromiak J 1999 Organogenesis of skeletal muscle in tissue culture *Methods Mol. Med.* **18** 217–25
- [23] Powell C A, Smiley B L, Mills J and Vandenburg H H 2002 Mechanical stimulation improves tissue-engineered human skeletal muscle *Am. J. Physiol. Cell Physiol.* **283** 1557–65
- [24] Boonen K J M, Rosaria-Chak K Y, Baaijens F P T, van der Schaft D W J and Post M J 2009 Essential environmental cues from the satellite cell niche: optimizing proliferation and differentiation *Am. J. Physiol. Physiol.* **296** C1338–45
- [25] Gholobova D, Gerard M, Terrie L, Desender L, Shansky J, Vandenburg H and Thorrez L 2019 Co-culture method to

Q2



- obtain endothelial networks within human tissue-engineered skeletal muscle *Myogenesis* 169–83
- [26] Shcherbakova D, Baloban M, Emelyanov A, Brenowitz M, Guo P and Verkhusha V 2016 Bright monomeric near-infrared fluorescent proteins as tags and biosensors for multiscale imaging *Nat. Commun.* **7** 1–12
- [27] Geraerts M, Micheils M, Baekelandt V, Debysers Z and Gijssbers R 2005 Upscaling of lentiviral vector production by tangential flow filtration *J. Gene Med.* **7** 1299–310
- [28] Ibrahim A et al 2009 Highly efficient multicistronic lentiviral vectors with peptide 2A sequences *Hum. Gene Ther.* **20** 845–60
- [29] Lendrum A C, Fraser D S, Slidders W and Henderson R 1962 Studies on the character and staining of fibrin *J. Clin. Pathol.* **15** 401–13
- [30] Carpentier G 2012 Angiogenesis Analyzer for Image—Gilles Carpentier Research Web Site: Computer Image Analysis
- [31] Gholobova D, Gerard M, Decroix L, Desender L, Callewaert N, Annaert P and Thorrez L 2018 Human tissue-engineered skeletal muscle: a novel 3D in vitro model for drug disposition and toxicity after intramuscular injection *Sci. Rep.* 1–14
- [32] Pfaffl M W, Horgan G W and Dempfle L 2002 Relative expression software tool (REST) for group-wise comparison and statistical analysis of relative expression results in real-time PCR *Nucleic Acids Res.* **30** 36
- [33] Stratman A N, Malotte K M, Mahan R D, Davis M J and Davis G E 2009 Pericyte recruitment during vasculogenic tube assembly stimulates endothelial basement membrane matrix formation *Blood* **114** 5091–101
- [34] Vandenburg H, Shansky J, Benesch-Lee F, Barbata V, Reid J, Thorrez L, Valentini R and Crawford G 2008 Drug-screening platform based on the contractility of tissue-engineered muscle *Muscle Nerve* **37** 438–47
- [35] Costa-Almeida R, Granja P L, Soares R and Guerreiro S G 2014 Cellular strategies to promote vascularisation in tissue engineering applications *Eur. Cells Mater.* **28** 51–67
- [36] Laschke M W and Menger M D 2012 Vascularization in tissue engineering: angiogenesis versus inosculation *Eur. Surg. Res.* **48** 85–92
- [37] Morin K T and Tranquillo R T 2013 In vitro models of angiogenesis and vasculogenesis in fibrin gel *Exp. Cell Res.* **319** 2409–17
- [38] Madden L, Juhas M, Kraus W E, Truskey G A and Bursac N 2015 Bioengineered human myobundles mimic clinical responses of skeletal muscle to drugs *Elife* **4** 1–14
- [39] Wang L, Shansky J and Vandenburg H 2013 Induced formation and maturation of acetylcholine receptor clusters in a defined 3D bio-artificial muscle *Mol. Neurobiol.* **48** 397–403
- [40] Wragg N M, Mosqueira D, Blokpeol-Ferreras L, Capel A, Player D J, Martin N R W, Liu Y and Lewis M P 2019 Development of a 3D tissue-engineered skeletal muscle and bone co-culture system *Biotechnol. J.* **1900106** 1900106
- [41] Redd M A, Zeinstra N, Qin W, Wei W, Martinson A, Wang Y, Wang R K, Murry C E and Zheng Y 2019 Patterned human microvascular grafts enable rapid vascularization and increase perfusion in infarcted rat hearts *Nat. Commun.* **10**
- [42] Jain R K 2003 Molecular regulation of vessel maturation *Nat. Med.* **9** 685–93
- [43] Kalluri R 2003 Basement membranes: structure, assembly and role in tumour angiogenesis *Nat. Rev. Cancer* **3** 422–33
- [44] Poschl E, Brachvogel U, Schlötzer-Schrehard B, Saito K, Ninomiya Y and Mayer U 2004 Collagen IV is essential for basement membrane stability but dispensable for initiation of its assembly during early development *Development* **131** 1619–28
- [45] Carosio S, Barberi L, Rizzuto E, Nicoletti C, Del Prete Z and Musarò A 2013 Generation of eX vivo-vascularized Muscle Engineered Tissue (X-MET) *Sci. Rep.* **3** 1420
- [46] Brady M A, Lewis M P and Mudera V 2008 Synergy between myogenic and non-myogenic cells in a 3D tissue-engineered craniofacial skeletal muscle construct *J. Tissue Eng. Regen. Med.* **2** 408–17
- [47] Jeon J S, Bersini S, Whisler J A, Chen M B, Dubini G, Charest J L, Moretti M and Kamm R D 2014 Generation of 3D functional microvascular networks with human mesenchymal stem cells in microfluidic systems *Integr. Biol.* **6** 555–63
- [48] Sacharidou A, Stratman A N and Davis G E 2011 Molecular mechanisms controlling vascular lumen formation in three-dimensional extracellular matrices *Cells Tissues Organs* **195** 122–43
- [49] Gökçinar-Yagci B, Uçkan-Çetinkaya D and Çelebi-Saltik B 2015 Pericytes: properties, functions and applications in tissue engineering *Stem. Cell Rev. Rep.* **11** 549–59
- [50] Ding R, Darland D C, Parmacek M S and Amore P A D 2004 Endothelial-mesenchymal interactions in vitro reveal molecular mechanisms of smooth muscle/pericyte differentiation *Stem. Cells Dev.* **13** 509–20
- [51] Lesman A, Koffler J, Atlas R, Blinder Y J, Kam Z and Levenberg S 2011 Engineering vessel-like networks within multicellular fibrin-based constructs *Biomaterials* **32** 7856–69
- [52] Nör J E, Peters M C, Christensen J B, Sutorik M M, Linn S, Khan M K, Addison C L, Mooney D J and Polverini P J 2001 Engineering and characterization of functional human microvessels in immunodeficient mice *Lab. Invest.* **81** 453–63
- [53] Van der Schaft D W J, Van Spreuwel A C C, Van Assen H C and Baaijens F P T 2011 Mechanoregulation of vascularization in aligned tissue-engineered muscle: a role for vascular endothelial growth factor *Tissue Eng. Part A* **17** 2857–65
- [54] Sriram G, Tan J Y, Islam I, Rufaihah A J and Cao T 2015 Efficient differentiation of human embryonic stem cells to arterial and venous endothelial cells under feeder- and serum-free conditions *Stem. Cell Res. Ther.* **6** 261
- [55] Van Beem R T, Verloop R E, Kleijer M, Noort W A, Loof N, Koolwijk P, Van der Schoot C E, Van Hinsbergh V W M and Zwaginga J J 2009 Blood outgrowth endothelial cells from cord blood and peripheral blood: angiogenesis-related characteristics in vitro *J. Thromb Haemost* **7** 217–26
- [56] Martin N R W, Aguilar-Agon K, Robinson G P, Player D J, Turner M C, Myers S D and Lewis M P 2017 Hypoxia impairs muscle function and reduces myotube size in tissue engineered skeletal muscle *J. Cell. Biochem.* **118** 2599–605
- [57] Shultz L et al 2010 Multiple defects in innate and adaptive immunologic function in NOD/LtSz-scid mice *J. Immunol.* **154** 180–91
- [58] Christianson S 1997 Enhanced human CD4+ T cell engraftment in beta2-microglobulin-deficient NOD-scid mice *J. Immunol.* **158** 3578–86
- [59] Yoshino H et al 2000 Natural killer cell depletion by anti-asialo GM1 antiserum treatment enhances human hematopoietic stem cell engraftment in NOD/Shi-scid mice *Bone Marrow Transplant.* **26** 1211–6
- [60] Xia Z, Ye H, Choong C, Ferguson D J P, Platt N, Cui Z and Triffitt J T 2004 Macrophagic response to human mesenchymal stem cell and poly( $\epsilon$ -caprolactone) implantation in nonobese diabetic/severe combined immunodeficient mice *J. Biomed. Mater. Res. Part A* **71** 538–48
- [61] Laumonier T and Menetrey J 2016 Muscle injuries and strategies for improving their repair *J. Exp. Orthop* **3** 15
- [62] Juhas M, Abutaleb N, Wang J T, Ye J, Shaikh Z, Sriworarat C, Qian Y and Bursac N 2018 Incorporation of macrophages into engineered skeletal muscle enables enhanced muscle regeneration *Nat. Biomed. Eng.* **2** 942–54
- [63] Sadtler K et al 2016 Developing a pro-regenerative biomaterial scaffold microenvironment requires T helper 2 cells *Science (80-)* **352** 366–70
- [64] Gilbert-Honick J, Iyer S R, Somers S M, Lovering R M, Wagner K, Mao H Q and Grayson W L 2018 Engineering functional and histological regeneration of vascularized skeletal muscle *Biomaterials* **164** 70–79

- [65] Zhang M, Methot D, Poppa V, Fujio Y, Walsh K and Murry C E 2001 Cardiomyocyte grafting for cardiac repair: graft cell death and anti-death strategies *J. Mol. Cell. Cardiol.* **33** 907–21
- [66] Kaully T, Kaufman-Francis K, Lesman A and Levenberg S 2009 Vascularization—the conduit to viable engineered tissues *Tissue Eng. Part B: Rev.* **15** 159–69
- [67] Kaijzel E L, Koolwijk P, Van Erck M G M, Van Hinsbergh V W M and De Maat M P M 2006 Molecular weight fibrinogen variants determine angiogenesis rate in a fibrin matrix in vitro and in vivo *J. Thromb Haemost* **4** 1975–81
- [68] White S, Pittman C, Hingorani R, Arora R, Esipova T, Vinogradov S, Hughes C, Choi B and George S 2014 Implanted cell-dense prevascularized tissues develop functional vasculature that supports reoxygenation after thrombosis *Tissue Eng. Part A* **20** 2316–28
- [69] Wolbank S, Pichler V, Crawford J F, Meinel A, van Griensven M, Goppelt A and Redl H 2015 Non-invasive in vivo tracking of fibrin degradation by fluorescence imaging *J. Tissue Eng. Regen. Med.* **9** 973–6
- [70] Thorrez L, DiSano K, Shansky J and Vandenburg H 2018 Engineering of human skeletal muscle with an autologous deposited extracellular matrix *Front Physiol.* **9** 1–11
- [71] Rahimi N, Swennen G, Verbruggen S, Scibiorek M, Molin D G and Post M J 2014 Short Stimulation of Electro-Responsive PAA/Fibrin Hydrogel Induces Collagen Production *Tissue Eng. Part C: Methods* **20** 703–13
- [72] Daub J T and Merks R M H 2013 A Cell-Based Model of Extracellular-Matrix-Guided Endothelial Cell Migration During Angiogenesis *Bull. Math. Biol.* **75** 1377–99
- [73] Van Linthout S, Miteva K and Tschöpe C 2014 Crosstalk between fibroblasts and inflammatory cells *Cardiovasc. Res.* **102** 258–69
- [74] Bloise N et al 2018 Ether-oxygen containing electrospun microfibrillar and sub-microfibrillar scaffolds based on poly(butylene 1,4-cyclohexanedicarboxylate) for skeletal muscle tissue engineering *Int. J. Mol. Sci.* **19** 3212
- [75] Yuan T, Xiao Y, Fan Y, Liang J and Zhang X 2017 The degradation and local tissue effects of collagen hydrogel and sponge implants in muscle *Polym. Test* **62** 348–54